FINAL REPORT

NASW-3770

GRAVITY ANOMALY MAP OF MARS AND MOON AND ANALYSIS OF VENUS GRAVITY FIELD: NEW ANALYSIS PROCEDURES

Carl Bowin, Principal Investigator

Woods Hole Oceanographic Institution
Woods Hole, MA 02543

FINAL REPORT

NASW-3770

GRAVITY ANOMALY MAP OF MARS AND MOON AND ANALYSIS OF VENUS GRAVITY FIELD: NEW ANALYSIS PROCEDURES

INTRODUCTION

Gravity anomalies are important for exploring the interior structure and mass distribution within a planet. More than ten million gravity measurements have been made on the earth's surface, eleven measurements on the moon's surface, and none by instruments on the surface of any other planetary body. Orbiting satellites indicate broad gravity anomaly patterns by the perturbations of their orbit paths. These patterns are usually analyzed using sets of spherical harmonic coefficients calculated from orbit perturbation data. Examples for the earth are GEM-9 (Lerch, et al., 1979) and GEM-L2 (Lerch, et al., 1982). Ananda et al. (1980); Bills (1982); Williams et al. (1983) and Mottinger et al. (1983) include spherical harmonic solutions for Venus. These solutions include information on the long wavelength portion of the gravity spectrum only.

More detailed information on planetary gravity fields is contained in the Doppler residual data from radio tracking of spacecraft. The acceleration (gravity) anomaly estimates determined from Doppler residuals are for components of the gravity field directed along the spacecraft-earth line. When that line defines a vector directed towards the center of Venus or another planetary body, the residual line-of-sight (LOS) acceleration observation is almost equivalent to the radial gravity anomaly at that location. The least squares filtering procedures applied to the Doppler data to obtain the LOS results reduce the true absolute amplitudes of the acceleration vectors (Gottlieb, 1970). The preparation of gravity anomaly

maps and analysis of the planetary gravity field directly from the LOS data have been hampered until now by being varied mixtures of radial, tangential, and intermediately-directed components of acceleration depending upon where the earth happened to be at the time of the measurement and occurring at varying altitudes above the planet surface.

A method for estimating radial gravity anomalies from LOS acceleration data, their interpolation, and use of iteration for improved radial estimates was outlined by Bowin (1983); a preliminary radial gravity anomaly map of Venus at spacecraft altitude was presented, and mass anomalies of the surface structures were shown to be the most significant contributors to the gravity field of Venus. In search of an appropriate means to invert the first radial gravity estimate to geoid anomalies for the proposed iteration method (Bowin, 1983), we encountered the technique of harmonic splines which allows direct estimation of the complete gravity field (geoid, gravity, and gravity gradients) everywhere over the planet's surface from the LOS vector data. This paper presents the harmonic spline results as a series of maps of Venus at spacecraft and constant altitudes. Global (except for polar regions) and local relations of gravity to topography are described.

HARMONIC SPLINES

The method of analysis we have chosen here is that of harmonic splines which has been discussed in detail and applied in previous and current studies in geomagnetism (Shure, Parker and Backus 1982; Parker and Shure, 1982; Shure, Whaler, Gubbins and Hobbs, 1983). To apply the exact method is computationally unfeasible. It requires the solution of a square system of equations which has dimensions equal to the number of data (D). Since there are approximately 140,745 points over most of Venus between -45 and +70 latitude, manipulation of a matrix of nearly 20 billion elements would be required for the most rigorous

solution. Even the reduced LOS data set of 9,364 measurements used in this study would require manipulation of a system of over 87 million elements which also is not practical with our computers. A modification in which the number of basis functions is reduced (to P) requires the solution of a D x P system, then iteratively P x P systems. The resolution at the planet's surface resulting from reducing the model to a few hundred of these functions would be about 5000 km. Clearly, the data have more detailed valuable information, thus leading us to a piecewise solution instead of a more satisfying single global solution. In this piecewise solution, we find models region by region which are piecewise harmonic and optimally smooth. In our experience, the choice of smoothness criterion has far less influence on the models produced than the amount of misfit allowed. We seek models of Venus, Mars and the moon which minimize the rms gravity subject to the data constraints. In any given region modeled we use a representative abstracted set of the data but fit only a subset of the optimal solution's set of functions; because of the data density many of these functions are nearly redundant. The model found is then sub-optimal, but nearly optimal area by area and therefore in total. Given the piecewise model it is now possible to upward and downward continue the field quantities desired with a few parameters unlike some other methods which must return to the full dataset for each desired calculation. Details about areas and numbers of knots used for the solution presented for Venus are discussed in a later section. If one wishes to examine a specific area on a planet's surface, the logical way to proceed is to model a large enough subset of the global dataset centered on that area which would not then suffer from the edge effects of piecing together solutions for adjacent areas. We show an example of this procedure for the moon's orientale region.

VENUS: APPLICATION OF THE METHOD OF HARMONIC SPLINES

We will briefly sketch here the harmonic spline method in the context of LOS measurements (gravitational acceleration along a given direction from which the central-body term has been subtracted).

The measurements are $\gamma_j = \underline{0}_j \cdot \underline{\gamma}(\underline{r}_j) = -\underline{0}_j \cdot \nabla T \qquad j=1,2...N \qquad [1]$

where $\underline{r}_j$ is the measurement location, γ_j is the gravity anomaly in the direction of line-of-sight $\underline{0}_j$. The potential T satisfies Laplace's equation $\nabla^2 T=0$ outside of the planet. Unfortunately, downward continuation of observations from satellite altitudes can result in very large and irregular fields because of the enhancement of short-wavelength errors. To minimize this problem we find the smoothest surface field consistent with the observations. We have some flexibility in choosing the measure of smoothness and opt to express it as a positive integral taken over the planet's surface. The functional we have chosen to quantify the field's roughness is

$$F[\underline{f}] = \int_{|\underline{r}|>r_o} |\underline{f}(\underline{r})|^2 \, dV \qquad [2]$$

where r_o is the radius of the planet (assumed to be spherical) and F is proportional to the energy in the anomalous gravity field ($\underline{f} = -\nabla T$) stored outside the planet.

This problem may now be viewed as a linear inverse problem which can be cast into the usual Hilbert space formulation. We first state, without proof, some basic results and refer readers interested in more detail to the original papers on harmonic splines (Shure, Parker and Backus, 1982; Parker and Shure, 1982) as well as to Parker (1977) for a general review of inverse theory. The relation (1) may be rewritten as

$$\gamma_j = \langle \underline{e}_j , \underline{f} \rangle \qquad [3]$$

where $\langle \cdot, \cdot \rangle$ denotes the inner product in the chosen Hilbert space. There is then a unique norm-minimizing model $\underline{f}_o$ which consists of a linear combination of the $\underline{e}_j$ according to

$$\underline{f}_o = \sum_{j=1}^{N} \alpha_j \underline{e}_j \qquad [4]$$

where the coefficients α_j are given by

$$\alpha_j = \sum_{k=1}^{N} (\Gamma^{-1})_{jk} \gamma_k \qquad [5]$$

and Γ is the Gram matrix of inner products:

$$\Gamma_{jk} = \langle \underline{e}_j , \underline{e}_k \rangle \qquad [6]$$

For definiteness, a Cartesian axis system is introduced, with origin at the planet's center of mass, z along the rotation axis and x through the 0° meridian; all field components in this section are referred to this frame which should not be confused with the local one often used. At any point outside the planet, a given component of the model, for example x, can be computed by

$$\gamma_x = \underline{\hat{0}}_x \cdot \underline{\gamma}(\underline{r}) = \langle \underline{e}_x , \underline{f}_o \rangle = \sum_{j=1}^{N} \alpha_j \langle \underline{e}_x , \underline{e}_j \rangle \qquad [7]$$

This shows how the field is calculated from the model, interpolating between the original points of observation.

We now consider the specific smoothness criterion (2) and note that with the divergence theorem this may be rewritten

$$F[\underline{f}] = \int T \, \underline{n} \cdot \nabla T \, dS \qquad [8]$$

where $\underline{n}$ is the outward unit vector normal to the surface. The spherical harmonic representation of T is exactly analogous to one for an external magnetic field

$$T(r,\theta,\phi) = r_o \sum_{\ell=1}^{\infty} \sum_{m=-\ell}^{\ell} f_\ell^m \, (r_o/r)^{\ell+1} \, Y_\ell^m(\theta,\phi) \qquad [9]$$

where the usual polar coordinate system is introduced, with θ as colatitude, ϕ longitude, and Y_ℓ^m are fully normalized complex spherical harmonics with $\int |Y_\ell^m|^2 d\omega = 1$ (Jackson, 1962), with the expansion referred to radius r_o. In terms of f_ℓ^m, (7) may be expressed as

$$F[\underline{f}] = \sum_{\ell=1}^{\infty} \sum_{m=-\ell}^{\ell} (\ell+1) \, |f_\ell^m|^2 = \sum_{\ell,m} (\ell+1) \, |f_\ell^m|^2 \qquad [10]$$

It is this relationship, which may be used as the basis for the inner product, which lies at the heart of the Hilbert space formulation. This linear vector space contains elements composed of an infinite ordered sequence of complex numbers; if $\underline{f}$ is in this space then

$$\underline{f} = \{f_1^{-1}, f_1^0, f_1^1 f_2^{-2}, f_2^{-1}, f_2^0, f_2^1, f_2^2 \ldots\}$$

The inner product of two elements $\underline{a},\underline{b}$ in the space is defined by

$$\langle \underline{a}, \underline{b} \rangle = \sum_{\ell,m} (\ell+1) \, a_\ell^m \, (b_\ell^m)^* = \langle \underline{b}, \underline{a} \rangle^*$$

and the induced norm $\|\underline{a}\| = \langle \underline{a},\underline{a} \rangle^{1/2}$. Membership in this space is restricted to elements with bounded norm.

Observations consist of components of the anomalous gravity above the planet. The relation between the model and the observations is shown in (1). What remains to be calculated are matrix elements Γ_{ij}.

$$\Gamma_{ij} = \underline{\hat{0}}_i^T \cdot \overline{K}(\underline{r}_i,\underline{r}_j) \cdot \underline{\hat{0}}_j \qquad [11]$$

where $\overline{K}(\underline{r},\underline{s})$ is a 3x3 second-rank tensor

$$\overline{K}(\underline{r},\underline{s}) = \frac{r_o^2}{4\pi} \underline{\nabla}_r \underline{\nabla}_s Q\left(\frac{r_o^2}{|\underline{r}||\underline{s}|}, \underline{r}\cdot\underline{s}\right) \qquad [12]$$

$$T(r,\theta,\phi) = r_o \sum_{\ell=1}^{\infty} \sum_{m=-\ell}^{\ell} f_\ell^m \, (r_o/r)^{\ell+1} \, Y_\ell^m(\theta,\phi) \qquad [9]$$

where the usual polar coordinate system is introduced, with θ as colatitude, ϕ longitude, and Y_ℓ^m are fully normalized complex spherical harmonics with $\int |Y_\ell^m|^2 d\omega = 1$ (Jackson, 1962), with the expansion referred to radius r_o. In terms of f_ℓ^m, (7) may be expressed as

$$F[\underline{f}] = \sum_{\ell=1}^{\infty} \sum_{m=-\ell}^{\ell} (\ell+1) \, |f_\ell^m|^2 = \sum_{\ell,m} (\ell+1) \, |f_\ell^m|^2 \qquad [10]$$

It is this relationship, which may be used as the basis for the inner product, which lies at the heart of the Hilbert space formulation. This linear vector space contains elements composed of an infinite ordered sequence of complex numbers; if $\underline{f}$ is in this space then

$$\underline{f} = \{f_1^{-1}, f_1^0, f_1^1, f_2^{-2}, f_2^{-1}, f_2^0, f_2^1, f_2^2 \ldots\}$$

The inner product of two elements $\underline{a},\underline{b}$ in the space is defined by

$$\langle \underline{a}, \underline{b} \rangle = \sum_{\ell,m} (\ell+1) \, a_\ell^m \, (b_\ell^m)^* = \langle \underline{b}, \underline{a} \rangle^*$$

and the induced norm $\|\underline{a}\| = \langle \underline{a},\underline{a} \rangle^{1/2}$. Membership in this space is restricted to elements with bounded norm.

Observations consist of components of the anomalous gravity above the planet. The relation between the model and the observations is shown in (1). What remains to be calculated are matrix elements Γ_{ij}.

$$\Gamma_{ij} = \underline{0}_i^T \cdot \overline{\underline{K}} \, (\underline{r}_i, \underline{r}_j) \cdot \underline{0}_j \qquad [11]$$

where $\overline{\underline{K}} \, (\underline{r},\underline{s})$ is a 3x3 second-rank tensor

$$\overline{\underline{K}} \, (\underline{r},\underline{s}) = \frac{r_o^2}{4\pi} \, \underline{\nabla}_r \, \underline{\nabla}_s \, Q \left(\frac{r_o^2}{|\underline{r}||\underline{s}|}, \, \underline{r} \cdot \underline{s} \right) \qquad [12]$$

where $Q(\rho, \mu) = \sum_{\ell} \frac{2\ell+1}{\ell+1} \rho^{\ell+1} P_{\ell}(\mu)$

$$= \frac{2\rho}{\sqrt{1-2\mu\rho+\rho^2}} - \rho - \ln\left(\rho-\mu+\sqrt{1-2\mu\rho+\rho^2}\right) \qquad [13]$$

$$1-\mu$$

There are two problems with the method as outlined above. The first is related to finding α_j, the coefficients of the harmonic splines. From [5] we notice that an NxN system of equations must be solved to find the spline model. Secondly, there is, as yet, no accounting for noisy and inaccurate measurements. Both of these issues are dealt with in explicit detail by Parker and Shure (1982) and only the ideas of the depleted basis analysis will be sketched here.

The spline functions are smoothly varying and the splines corresponding to two near-by locations are very similar. Instead of using all the functions in [5], we select a subset of these functions (we do not throw away the corresponding measurements) which corresponds to a sparser data distribution. These locations associated with the splines functions are called the knots. We then seek to minimize [2] with only the functions corresponding to the depleted set of knots, called the depleted basis. Unless we are extremely lucky, the model found in this way will not fit all of the measurements exactly. This, however, is acceptable provided the misfit (calculated as the sum of the squares of the differences between the data and model predictions) is acceptable based on prior assessment of what the errors associated with the data are. If the misfit in this basis is too large, more functions must be added to model the data adequately. If the data are overfit it is possible to minimize [2] further by relaxing the fit criterion further. This is accomplished by the introduction of a Lagrange multiplier which, when varied, is responsible for the trade-off

between misfit and norm. The necessary mathematics and computational details are in Parker and Shure (1982).

As mentioned above, the Pioneer Venus Orbiter LOS data available consist of approximately 140,745 points over most of Venus between -45° and +70° latitude. Although basis reduction can be effective for a substantial reduction in the number of knots before the model starts to deteriorate (Parker and Shure, 1982), clearly such a large data set must be decimated before the harmonic spline matrix manipulation becomes feasible with computers currently available. To this end the data used in the computations were reduced to one point per two degrees square. The reduction does not alter the gravity results significantly, as the shorter wavelength variations are attenuated at spacecraft altitudes in the range of 150 km to 4000 km (Figure 1).

In order to minimize instability due to errors in data processing and decrease computation costs, duplicate orbits that covered the same zones of longitudes were removed from the data set. We found that by removing five or six clearly erroneous orbits a reasonably smooth map could be made. The orbits used, 111-174 and 418-602, provide coverage at all longitudes, and have less noise than other sets of orbits.

The harmonic spline solution was obtained piecewise, by dividing the planet surface into a grid, and using a different set of spline coefficients (about 25 knots per cell) to model the field in each grid cell. The cells used are shown in Figure 1; generally the data were retrieved from an area four times as large as each cell to calculate the central cell's coefficients. This procedure does, however, introduce some mismatch error between adjacent cells, seen as discontinuities in Figure 2, which compares LOS data for individual orbits with equivalent closely spaced (0.1 to 0.4 degree) values computed from the harmonic spline model. A smoothing technique was employed to

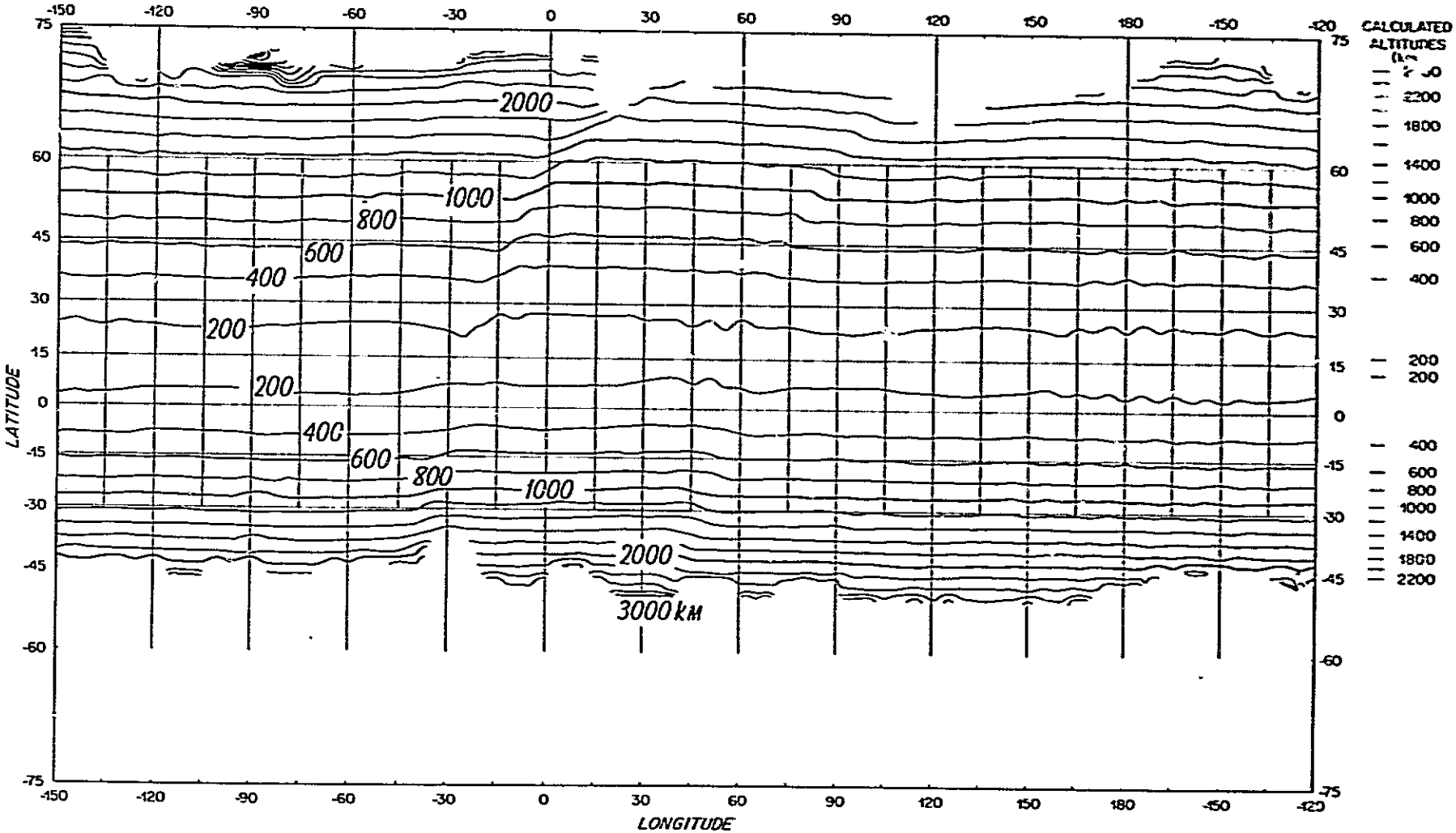

Fig. 1 Spacecraft average altitude for Pioneer Venus Orbiter for orbits 111 to 602. The grid lines indicate the cell boundaries used for the piecewise harmonic spline solution.

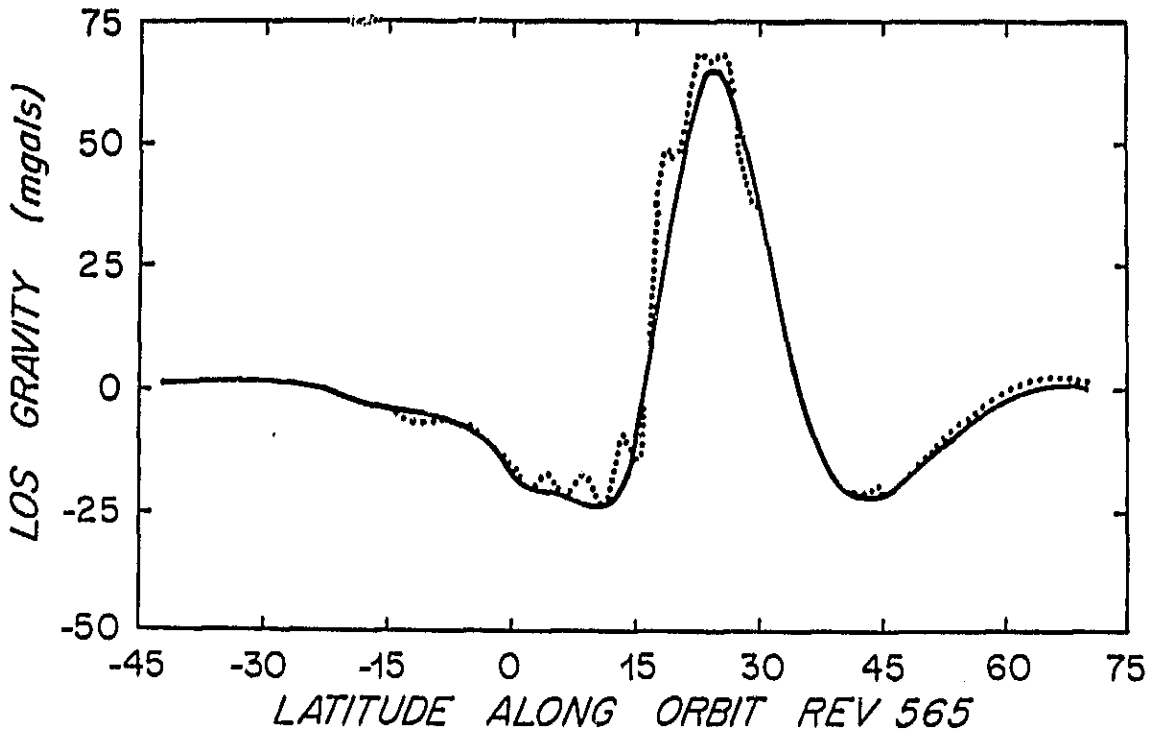

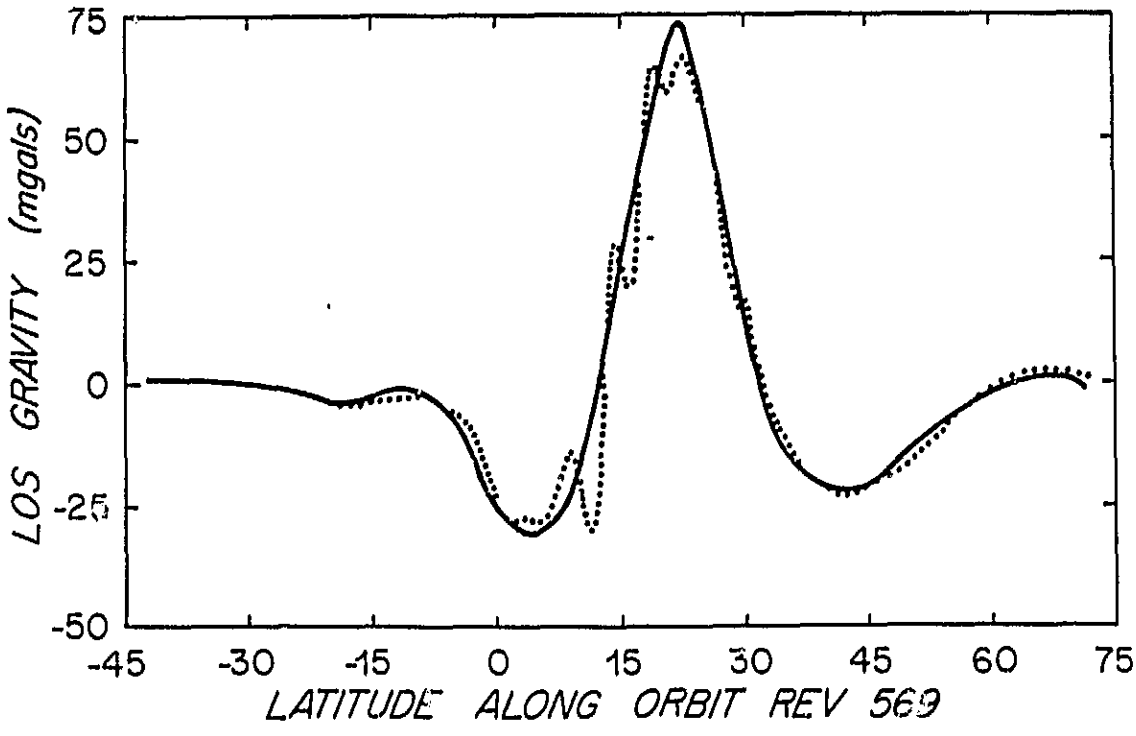

Fig. 2 Comparisons of measured LOS residual gravity anomaly with the gravity component in the LOS vector direction calculated from harmonic spline coefficients. Solid line is measured LOS values, and dashed line results from closely-spaced (0.1 to 0.4 degrees) calculated LOS values.

TABLE OF CONTENTS

alleviate some of the mismatch, in which the data used to calculate the model of each cell included artificial 'data' outside the cell edges, created from the coefficient sets of previously calculated, adjacent cells. Each of these additional, generated points was weighted more heavily than the LOS data in the harmonic spline modeling. We found, however, that this smoothing process tends to induce instability in cells that principally contain high-altitude data, and so we only used it for areas where the spacecraft altitude is low (between +30° and -15° latitude). The irregularities seen in Figure 2, which occur near cell boundaries indicate that features with half-wavelengths shorter than about 5° can not be resolved with the present model.

The harmonic spline approach in modeling LOS gravity does not depend upon choosing a source depth and configuration for causative mass anomalies as with point mass and disk modeling procedures with orbit simulation. However, by those modeling procedures (Phillips et al., 1978), a distorted gravity profile from the model could be compared with the similarly distorted residual LOS values, and hence harmonic spline models suggest a method for correcting for the reference level errors resulting from the least squares fitting procedure used to obtain the residual LOS values. Such a method is described at the end of this report. Harmonic splines automatically correct for the geometric distortion previously noted in LOS data by Bowin (1983) and Gottlieb (1970) such that maximum values are centered over the topographic feature, and not displaced to the side.

At each knot three weights were used. There are three because there are three independent functions associated with each knot due to the vector nature of the LOS measurements. We could instead have chosen a distribution of three times the number of knots with each using only one of the functions (chosen arbitrarily), but the models would be virtually indistinguishable. In fact,

this is an important advantage: in the model area, spline models are robust with respect to knot location. This is in marked contrast to point mass or disk models which are very sensitive to the location (especially depth) of the sources.

GRAVITY MAPS

With harmonic splines we can calculate gravity vectors at any altitude above the planet surface. To compare the harmonic spline method with prior results we first computed radial gravity at spacecraft altitude (Figure 3). That map agrees well with the radial gravity map prepared by Bowin (1983, Figure 7) between latitudes 60°N and 45°S, and both differ similarly from line-of-sight gravity maps at spacecraft altitude (eg. Sjogren et al., 1980, 1981, and 1983) by having better spatial correlation with topography in the region north of 30°N, and providing better estimates of vertical gravity anomalies. The two greatest positive gravity anomalies occur at Beta Regio (25°N, 80°W) and at Atla (5°N, 160°W), both of which are topographic highs that have been inferred to be sites of active volcanism (Bowin, 1983, p. 366). Both highs are flanked in the NE-SW direction, along the orbit paths, by negative anomalies that are largely due to the least squares filtering of the Doppler data (Gottlieb, 1970). The other lower-magnitude gravity highs in the band between 40°N and 15°S also correlate closely with locations of topographic highs. Note that the two discontinuities, parallel to orbit paths, crossing latitude 45°N at about -10° longitude and at about +75° longitude in the maps of LOS gravity data in Sjogren et al.(1983) and Bowin (1983), result from discontinuities in the viewing geometry and are not expressed in the harmonic spline results of Figure 3.

We have also computed the component of gravity along the LOS direction at spacecraft altitudes (Figure 1) along orbits 565 and 569 (Figure 2), both of

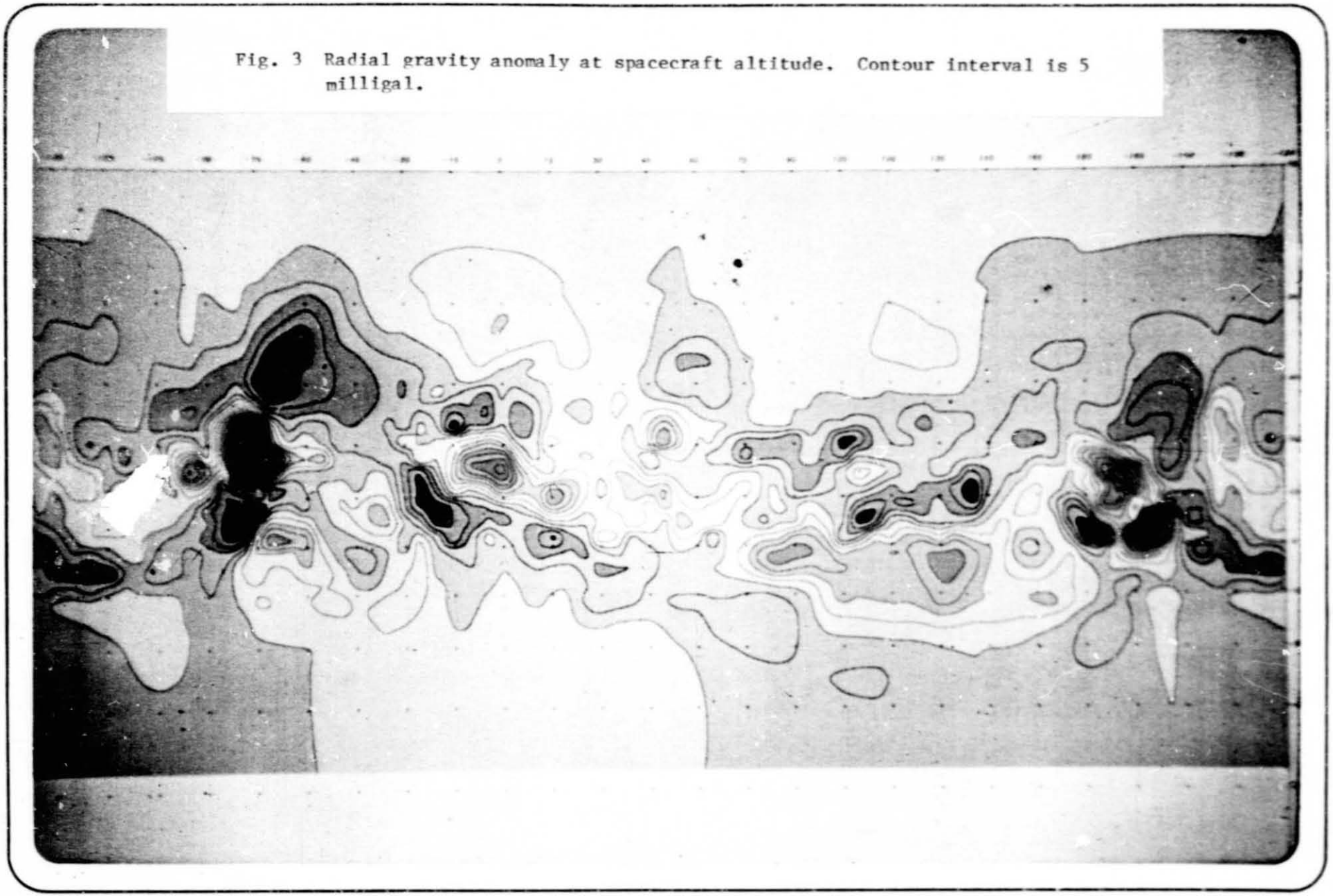

Fig. 3 Radial gravity anomaly at spacecraft altitude. Contour interval is 5 milligal.

which pass near Beta. The plots show that the harmonic spline results conform with the input data, although high-frequency 'noise' has been introduced at the cell boundaries where spacecraft altitude is low. Computation of tangential gravity components (Figures 4 and 5) verifies the model's internal consistency and numerical stability; horizontal zero lines coincide with locations of maxima and minima in the radial field (Figure 7).

Gravity data at constant altitude are more useful for analysis purposes than are data at varying spacecraft altitudes. Accordingly, radial gravity anomaly maps were prepared for 500 km (Figure 6) and 300 km (Figure 7) altitudes. In both of these maps, between 30°N and 15°S, the locations of the highs and lows are in close agreement with their locations in the map at spacecraft altitude (Figure 3). Their magnitudes differ, but in a manner consistent with their degree of upward or downward continuation from spacecraft altitude. In the region north of 30°N there is a marked improvement in the definition of gravity anomalies with respect to both the spacecraft altitude map of Figure 3 and to the map of Bowin (1983, Figure 7). The large positive anomaly between longitudes 45°W and 15°E is associated with the Ishtar continental mass, and the maximum near 65°N, 3°E is centered over Maxwell Montes, the highest topographic feature on Venus with nearly 12 km elevation. The other gravity maximum of Ishtar has not been well located because of sparse data coverage at the northern limits of the maps. The gravity high near 60°N and between 75°E and 145°E is in the vicinity of Tethus Regio. It is also apparent in the degree 7 (Williams, et al., 1983; Bowin, 1983, Figure 2) and degree 10 (Mottinger et al., 1983) gravity field spherical harmonic solutions for Venus, and thus it appears to be a real feature of the gravity field of Venus. Nearby, Tellus Regio (35°N, 80°E), however, has only a small positive anomaly relative to the adjacent plains.

ORIGINAL PAGE
COLOR PHOTOGRAPH

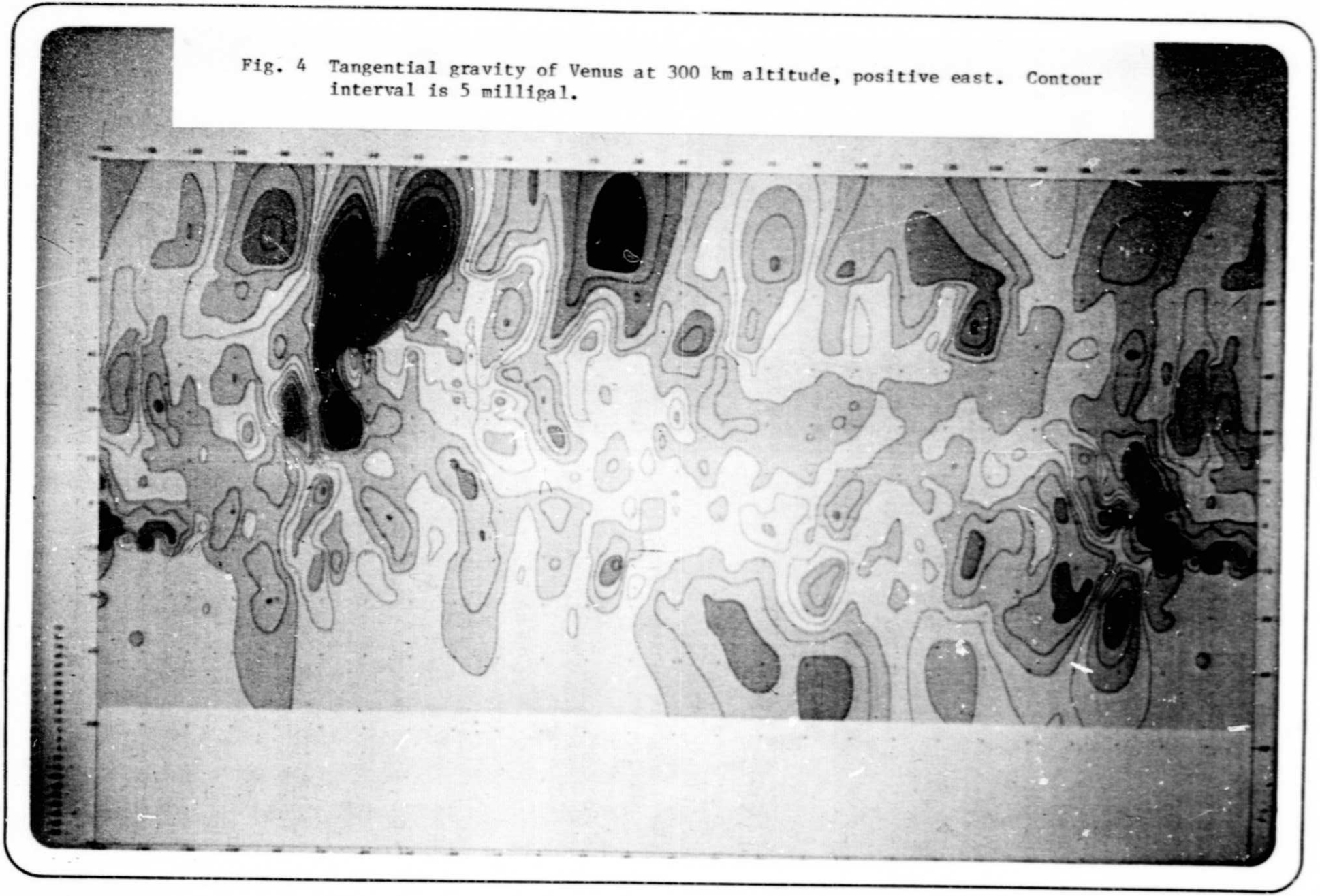

Fig. 4 Tangential gravity of Venus at 300 km altitude, positive east. Contour interval is 5 milligal.

ORIGINAL PAGE
COLOR PHOTOGRAPH

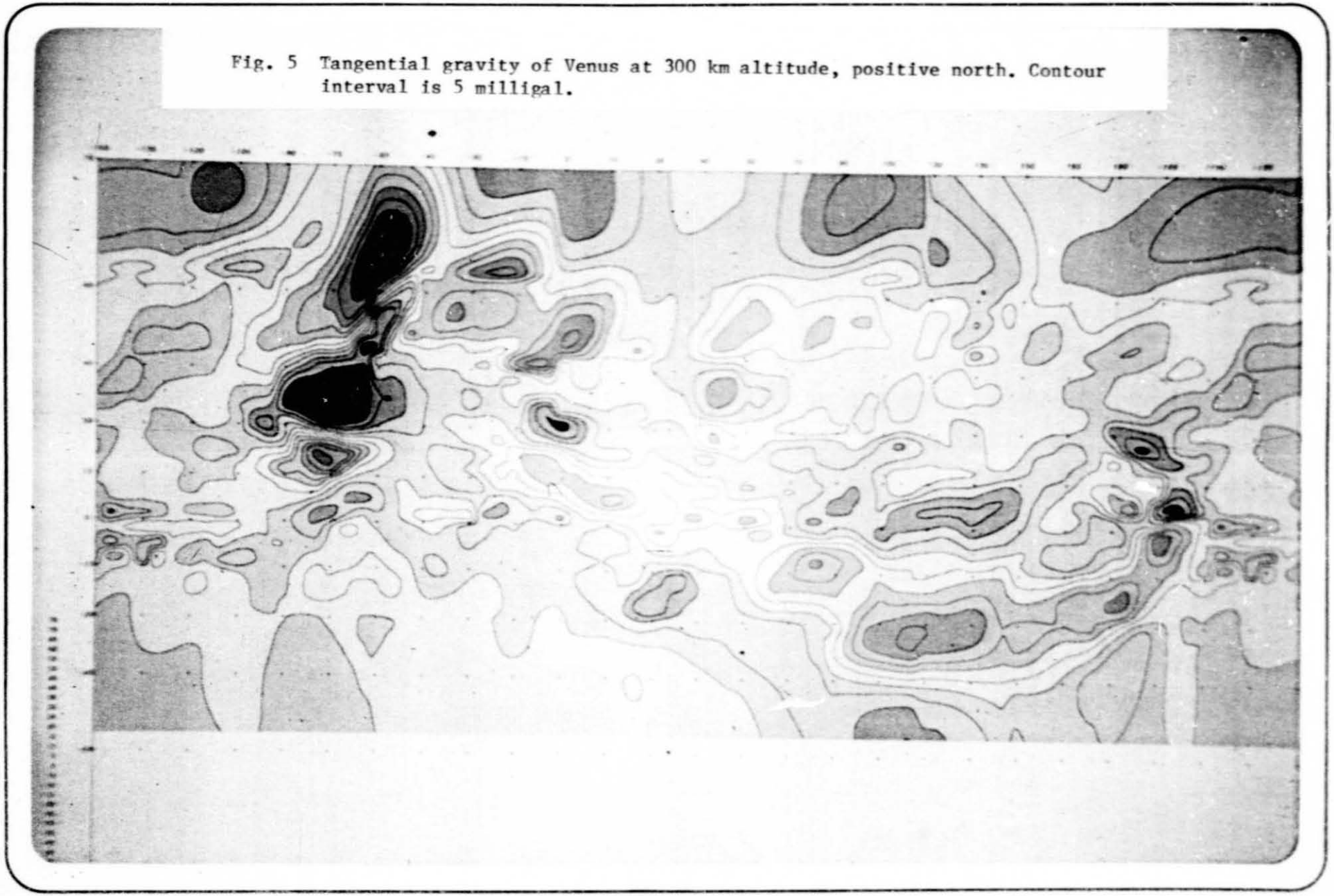

Fig. 5 Tangential gravity of Venus at 300 km altitude, positive north. Contour interval is 5 milligal.

ORIGINAL PAGE
COLOR PHOTOGRAPH

Fig. 6 Radial gravity anomalies of Venus at 500 km altitude. Contour interval is 5 milligal.

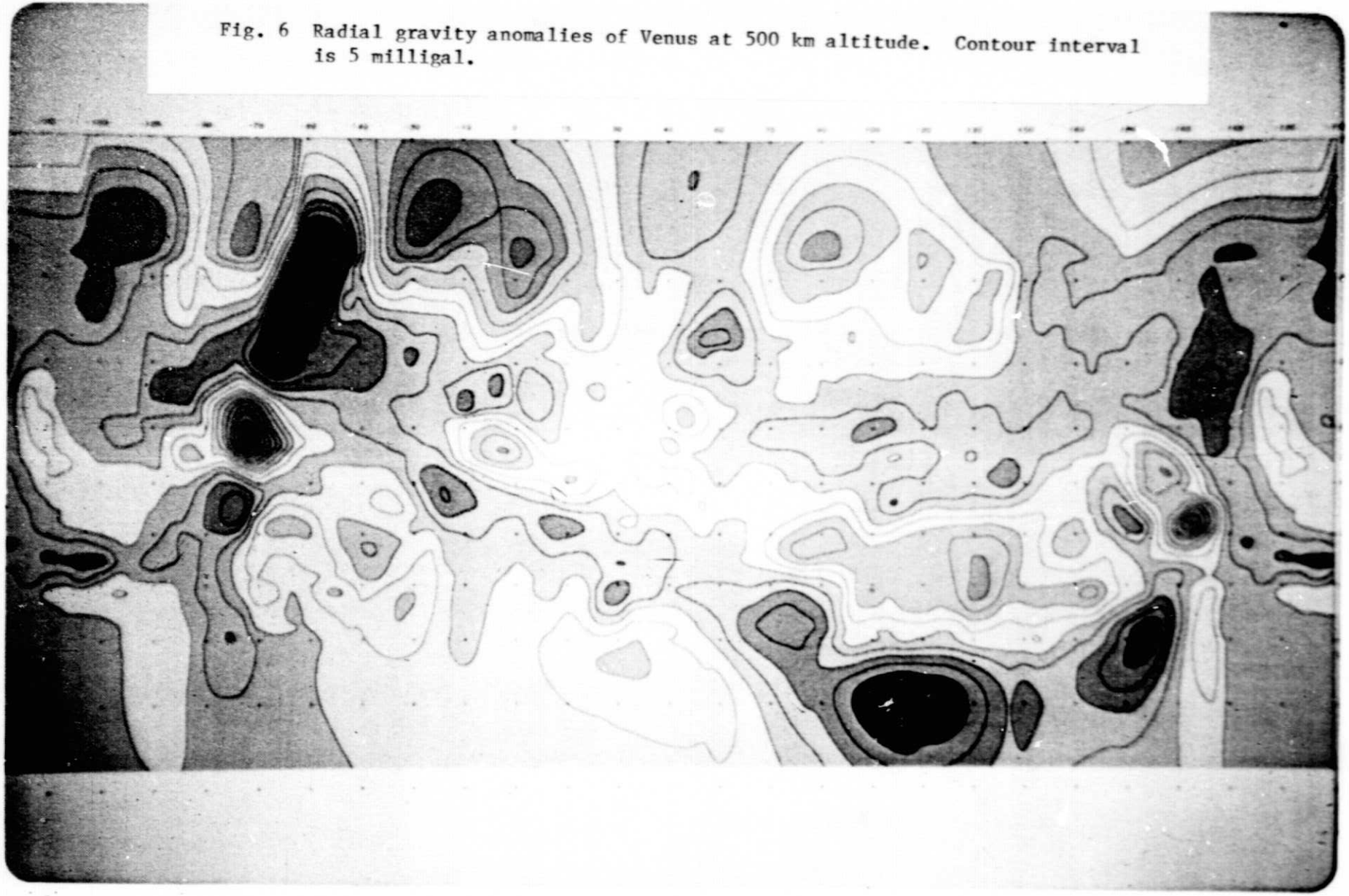

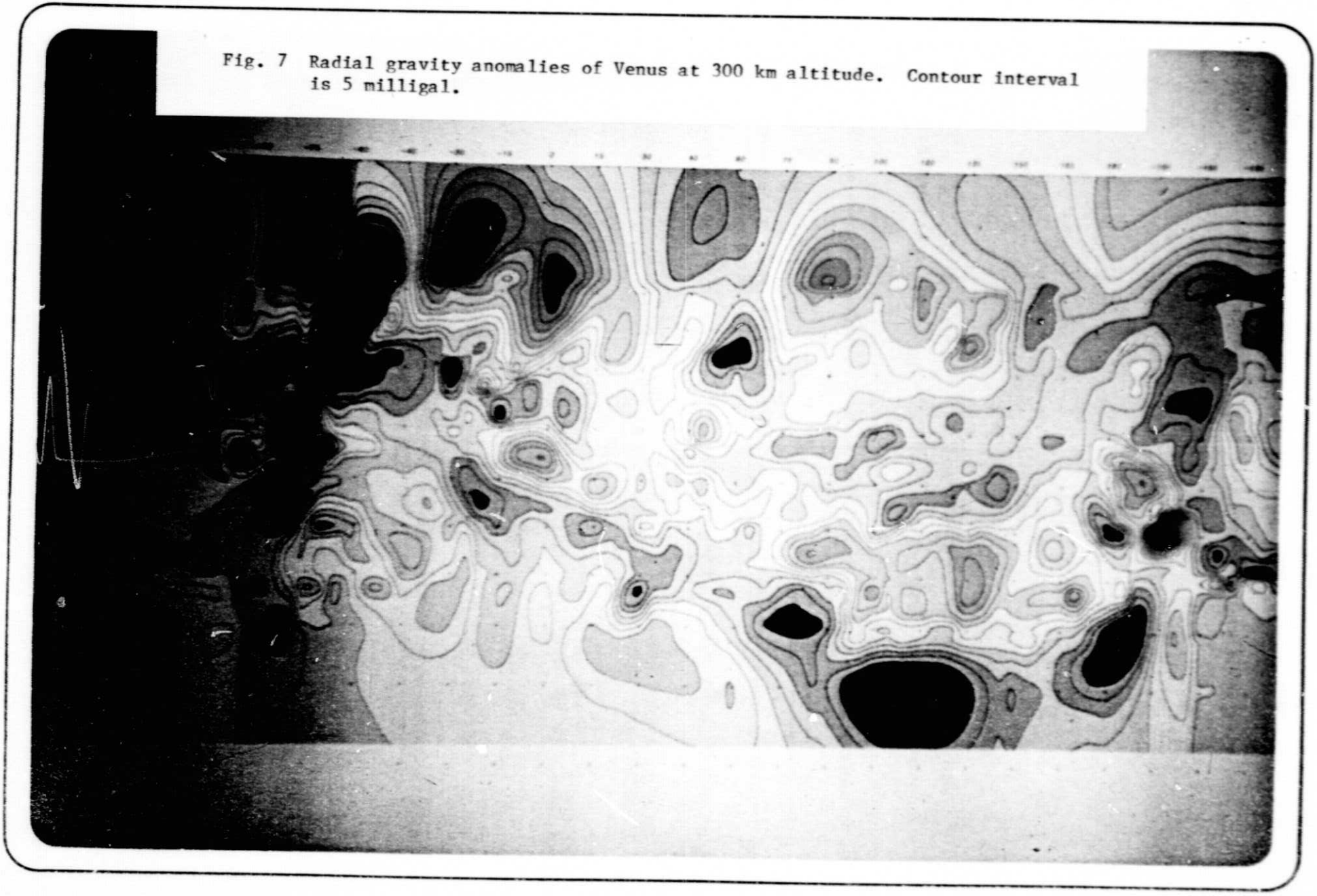

Fig. 7 Radial gravity anomalies of Venus at 300 km altitude. Contour interval is 5 milligal.

The most striking anomaly in both the 500 km and 300 km altitude gravity maps is the elongate negative anomaly east of north of Beta Regio. This anomaly is inferred to be an artifact of the least squares filtering procedure applied to the Doppler data cited previously. The two negative anomalies that flank the Beta positive along the orbit path direction are of about equal magnitude in the data at spacecraft altitude (Figure 3). The negative anomaly south of Beta has greater upward continuation in the 500 km altitude map than in the 300 km altitude map (Figure 8). Upward continuation attenuates the magnitudes of that anomaly. On the other hand, the negative anomaly north of Beta has significant downward continuation (amplification) at both 500 km and 300 km, due to the height of the spacecraft (Figure 8). Thus, in the constant altitude gravity maps shown, the negative anomaly north of Beta is amplified to magnitudes in excess of all other anomalies, indicating that that negative anomaly is principally an artifact of the initial processing procedure, rather than a real feature of the Venus gravity field. Note that the strong low at 45°S, south of Aphrodite, is farther from periapsis than Aphrodite itself, and accordingly has also been amplified more by downward continuation in the constant altitude map. The magnitude of the Aphrodite gravity high is much lower than that for Beta, and the induced flanking lows along the orbit path will have accordingly lower magnitudes than those for Beta Regio, as observed in the maps.

GEOID MAPS

Through appropriate manipulation, the harmonic spline model can provide estimates of geoidal undulations and tangential components of gravity, in addition to radial gravity. An example of this capability was shown previously (Figure 2) by the calculation of gravity along the LOS vector directions. We recognize that the term geoid refers strictly to the surface of the earth.

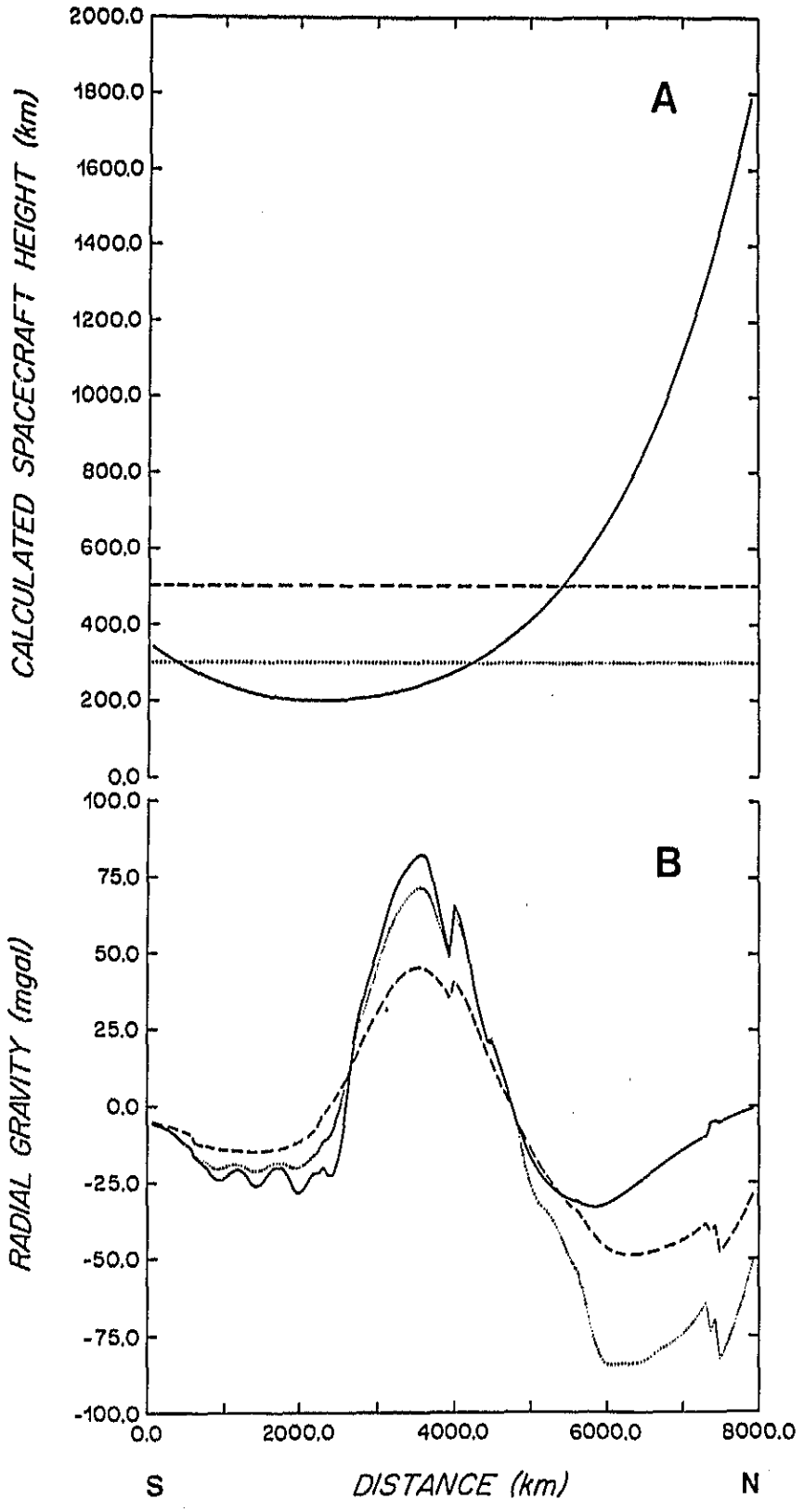

Fig. 8 Comparison of profiles of radial gravity anomaly at spacecraft, 500 km, and 300 km altitudes across Beta Regio in a direction parallel to the orbit paths. The line types in the height plot (A) provide identifications for the lines describing the gravity profiles (B).

However, we assume that its extended use to another planet and at altitudes above the surface will be understood in the absence of a suitable alternate term. A map of the geoidal undulations at 300 km altitude is given in Figure 9. The undulations are in meters referenced to a central body potential at an altitude of 300 km. This is the first detailed geoid anomaly map determined for Venus from LOS acceleration data. Previous geoidal maps have been prepared from sets of spherical harmonic models and have lower spatial resolution than those from harmonic splines. Note that the geoid map at 300 km altitude (Figure 9) has a close resemblance to the gravity map at 500 km (Figure 6), and that the gravity map at 300 km (Figure 7) has a higher-frequency anomaly pattern than does the geoid map at 300 km altitude.

On Venus, the major long-wavelength geoid and gravity anomalies each coincide with the locations of positive topographic features. On the earth, the major geoid anomalies do not coincide with locations of the earth's largest topographic features, including continents; the largest magnitude gravity anomalies occur at arc-trench systems and mountain ranges. These relations on the earth have been explained (Jordan, 1978; Bowin, 1983, in press) by mass anomalies in the core-mantle boundary region and lower mantle anomalies contributing most significantly to geoid anomalies, and lithosphere mass anomalies contributing most significantly to gravity anomalies. Thus, on Venus, major mass anomalies are apparently restricted to near the planet's surface since the geoid anomalies show very close correspondence to gravity and surface topographic anomalies. Thus, possible contributions from deep mass anomalies unrelated to surface structures must be minor.

GRAVITY-TOPOGRAPHY RELATIONS

On Venus, the geoid and gravity anomalies at 300 km altitude have significantly greater magnitude than corresponding anomalies for the earth.

ORIGINAL PAGE
COLOR PHOTOGRAPH

Fig. 9 Geoid undulations of Venus at 300 km altitude. Contour interval is 5 meters.

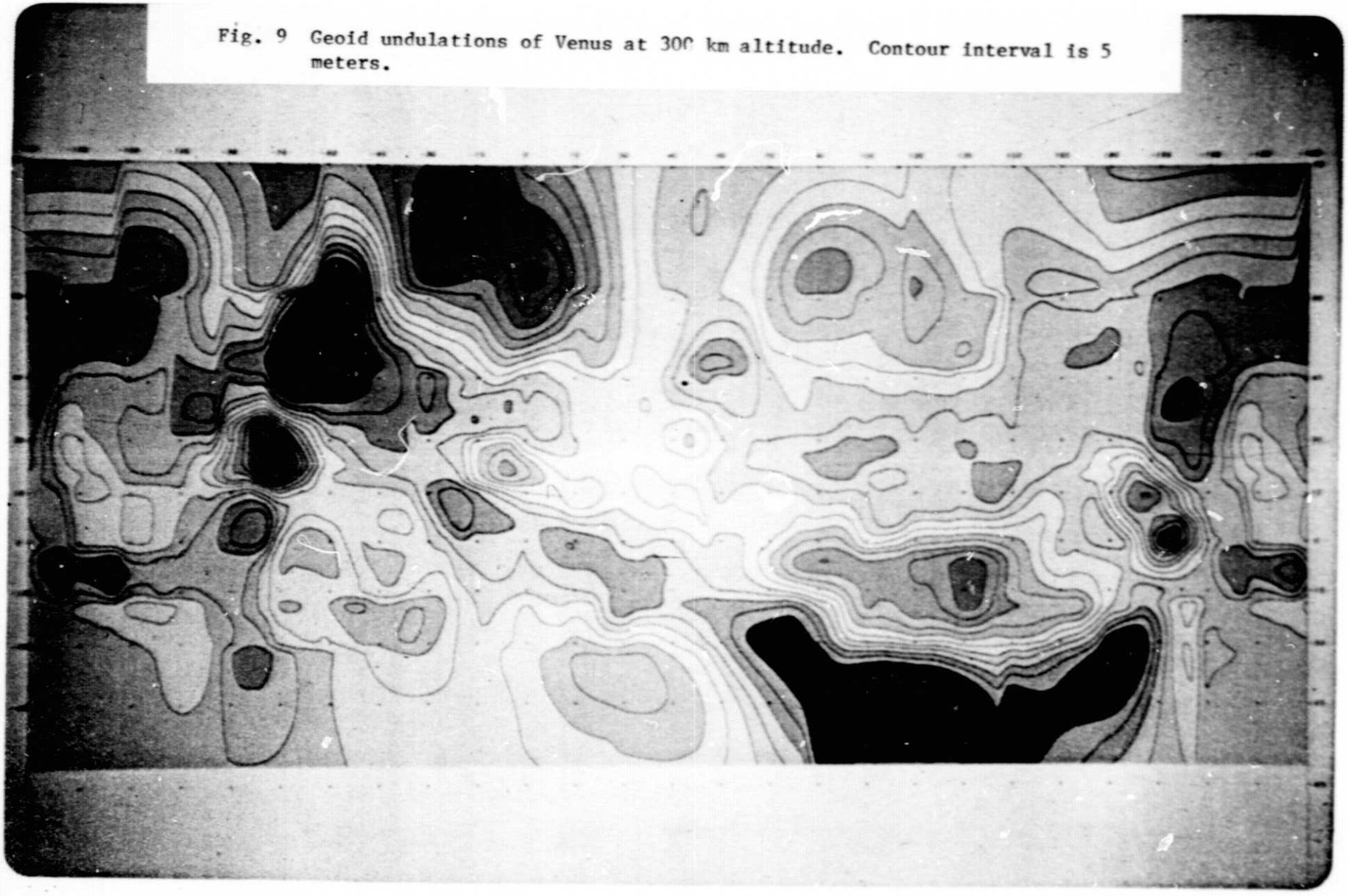

On the earth, free-air gravity anomalies are typically within ± 75 mgals of zero (Bowin et al., 1982) indicating that the earth's surface features are generally in isostatic equilibrium. At 300 km altitude the typical range is about ± 20 mgal (Figure 10). On Venus, the range of gravity anomalies at 300 km altitude is typically ± 25 mgal (Figure 11) and the range of geoid anomalies is typically 60 meters (Figure 12), and there is a positive correlation of anomalies with topographic height. Figure 11 shows scatter diagrams of radial gravity at 300 km altitude verses topographic height for the planet Venus between latitudes 70°N and -45°S. The data are from a grid of locations approximately equally spaced on the surface of the planet. The spacing is equivalent to five degrees of longitude at the equator. The gravity and geoid values are obtained from the harmonic spline model. The topographic values at each grid point are obtained by optimal estimation from the digital altimeter data provided by G.H. Pettengill and P. Ford. The optimal estimation uses objective mapping techniques (Gandin, 1965; Bretherton et al., 1976) but has been modified from Bowin (1983) to remove the altitude correction which does not apply to topography. The best fitting slopes for these data are 6.68 mgal/km topographic relief (Figure 11), and 7.2 meters of geoid anomaly/km topographic relief (not shown).

For the earth (Figure 10), spherical harmonic coefficients were used to compute gravity at 300 km altitude (GEM-9, Lerch, et al., 1979) and topography (Balmino et al., 1973 and Lee and Kaula, 1967). Note the bimodal clustering about 0 mgal at topographic heights of -4.5 and +0.25 km, near the two dominant peaks of the earth's hypsometric curve that result from the relief between ocean basins and continents. Aside from this relationship to the frequency of certain topographic heights, there is no obvious correlation of the gravity field from low harmonic degree (up to degree 10) with the earth's

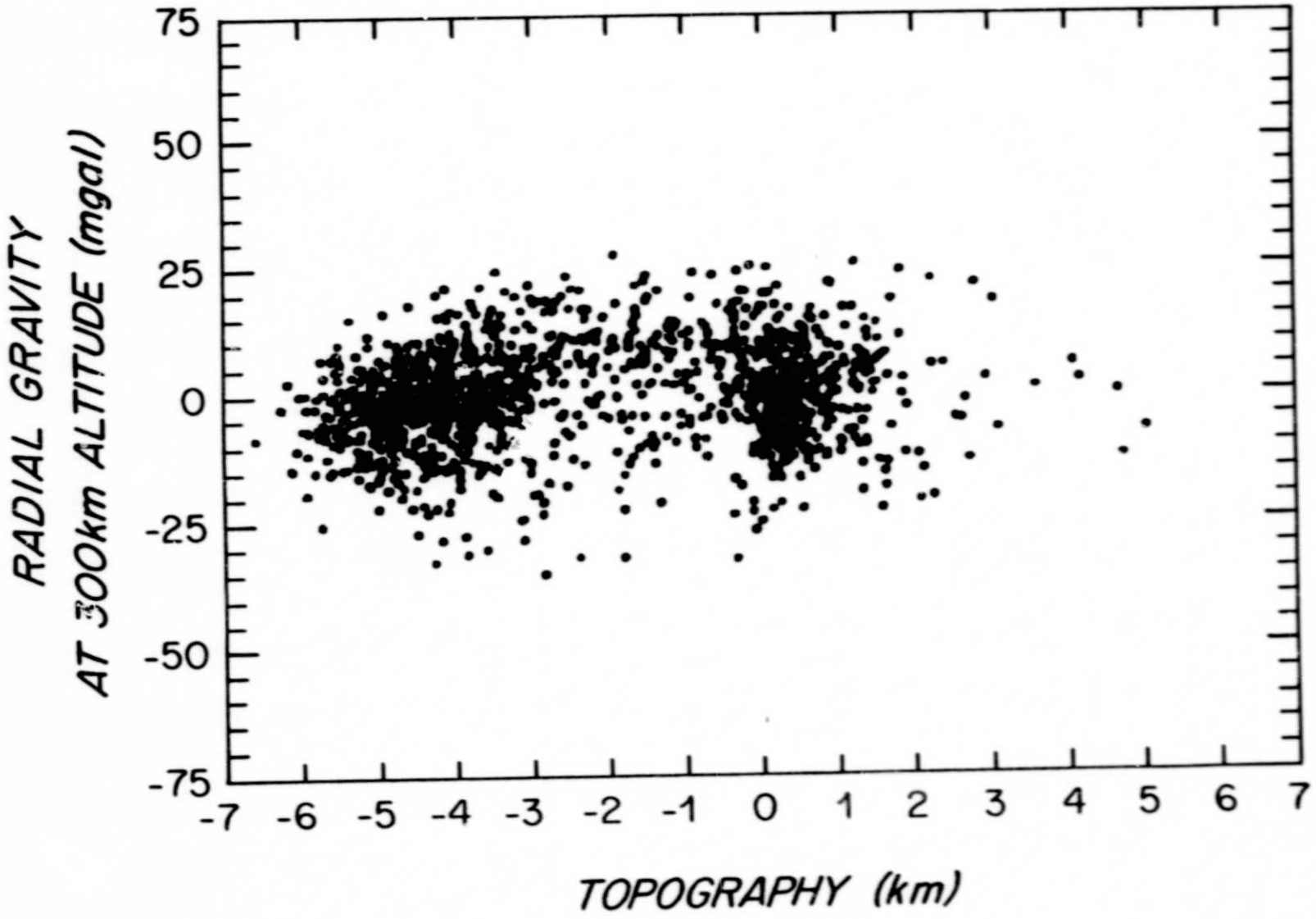

Fig. 10 Radial gravity at 300 km altitude versus surface topography for earth. Note the clustering about two depth ranges, one associated with oceanic depths and the other with continental shelves. Gravity from GEM-9 spherical harmonic coefficients (Lerch et al., 1979) and topography also from spherical harmonic coefficients (Balmino et al., 1973). Calculated at a set of locations equally spaced by about 5° on the surface. This set is also used for Figures 9 and 10.

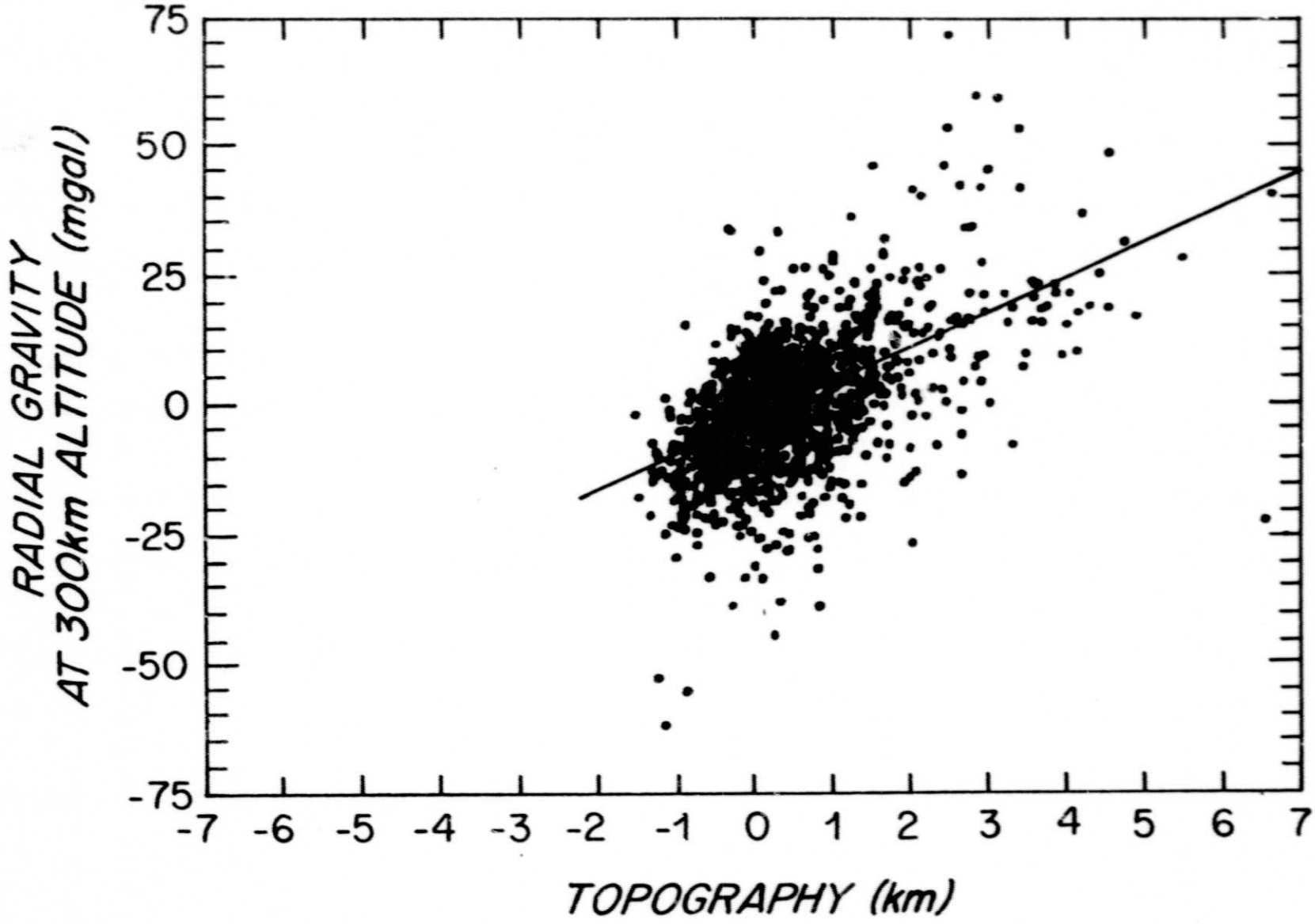

Fig. 11 Radial gravity at 300 km altitude versus surface topography for Venus. Note the definite positive correlation of anomalies with topographic height: RMS slope of 6.68 mgal/km. Gravity from harmonic spline results (this paper) and topography from Pioneer Venus digital altimeter data. Calculated at a set of locations equally spaced by about 5° on the surface. This set is also used for Figures 8 and 10.

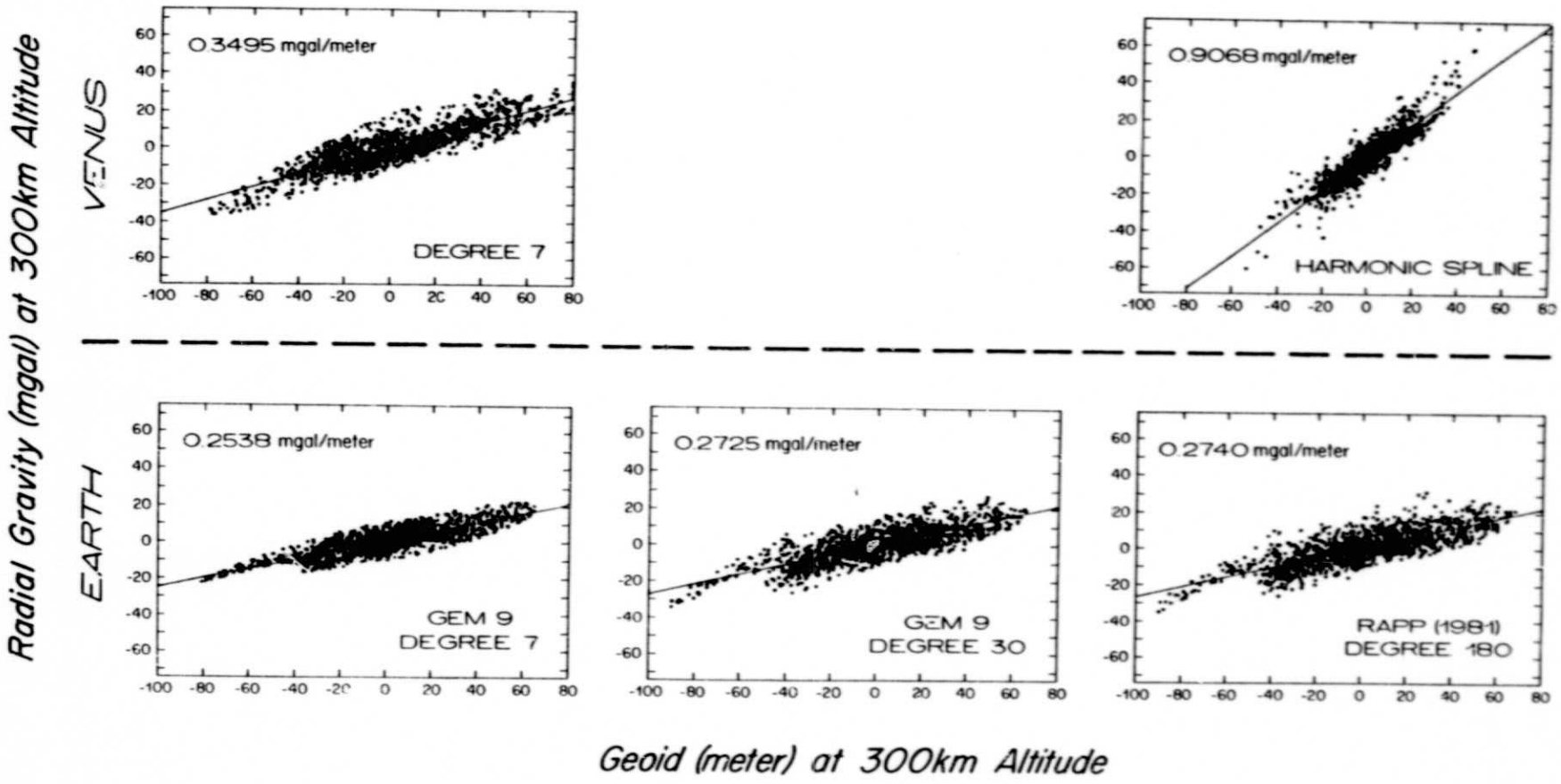

Fig. 12 Radial gravity anomaly versus geoid anomaly at 300 km altitude for Venus and earth.

surface topographic relief (Bowin, 1983, Figure 9c). This further demonstrates the marked contrast between the gravity relations on Venus (Figure 11) and those on the earth (Figure 10).

Although the total range of anomalies at 300 km altitude is similar for both the earth and Venus, their relationships to topographic features are markedly different. On the earth, the large broad gravity and geoid anomalies show little relationship to the locations of continents, the planet's largest topographic features. This is especially clear in geoid maps. Some spatial correspondence is observed in the western Cordillera of South and North America and the island of Iceland. On Venus, however, virtually all the positive gravity and geoid anomalies correlate well with positive topographic features, which results in the positive slope seen in Figure 11. This comparison is perhaps further support for the analyses of Jordan (1978) and Bowin (1983, in press) that over half the energy (variance) in the earth's geoid field arises from mass anomalies deeper than 600 km in the mantle and at the core-mantle boundary. For Venus the geoid and gravity anomalies appear to be due principally to mass anomalies associated with surface topographic features. Thus, mass anomalies in about the outer 600 km (26.9% of volume) of Venus are inferred to be the source for its geoid and gravity anomalies, whereas the earth's geoid and gravity anomalies may result from mass anomalies in the outer 2900 km (83.8% of volume) of the planet. If the mass anomalies of Venus occur principally in the outer 200 km, as we suggest later in this report, then Venus' geoid and gravity anomalies principally arise from only 9.6% of the volume of the planet.

Bowin (1983, in press) showed that the ratio of gravity anomaly to geoid anomaly values at the center of an anomaly feature provides an estimate of the maximum possible source depth. Directly above a point mass at depth, Z, the

gravity anomaly is $g=GM/Z^2$ where G is the gravitational constant and M the anomalous mass. The geoid height, N, is related to anomalous potential, T, by Brun's formula so that $N=T/g_o$ or $N=GM/g_oZ$ with g_o being the normal gravity for the planet. Thus the ratio of the gravity anomaly to the geoid anomaly directly above a point mass at depth Z is: $g/N=g_o/Z$. Conversely, the depth can be determined by: $Z=g_o/(g/N)$. Since point mass models indicate the maximum possible depth for the source of a mass anomaly, the g/N ratio provides an estimate of the maximum source depth. Low ratio values (<1.0 mgal/m) indicate deep maximum depths, but they may also result from an anomalous mass being very broadly distributed at a shallow depth or at the surface. Gravity to geoid ratio values at 300 km altitude above both Venus and the earth are displayed in Figure 12. These data were determined from sets of spherical harmonic coefficients for Venus and the earth, and from the harmonic spline model of this paper. Note that in both the degree 7 comparison and the comparison of the highest available resolution data sets (harmonic spline results for Venus and Rapp's 180 degree spherical harmonic coefficients for earth), greater gravity to geoid ratio values occur on Venus. If mass anomalies within Venus were distributed similarly to those of the earth, then the ratio of gravity to geoid on Venus should be slightly smaller, rather than greater. This is because the ratio of gravity to geoid for each individual spherical harmonic degree (Bowin, 1983, Eqn. 8, p. 69) is expected to be 0.945 smaller for Venus at 300 km above the surface. The larger observed gravity to geoid ratio values on Venus (Figure 12), therefore, are additional evidence for a different and shallower distribution of anomalous mass on Venus compared to that on the earth.

We now examine the gravity anomalies for different areas of Venus. Gravity to topography relations for twelve regions (Figure 13) on Venus with positive

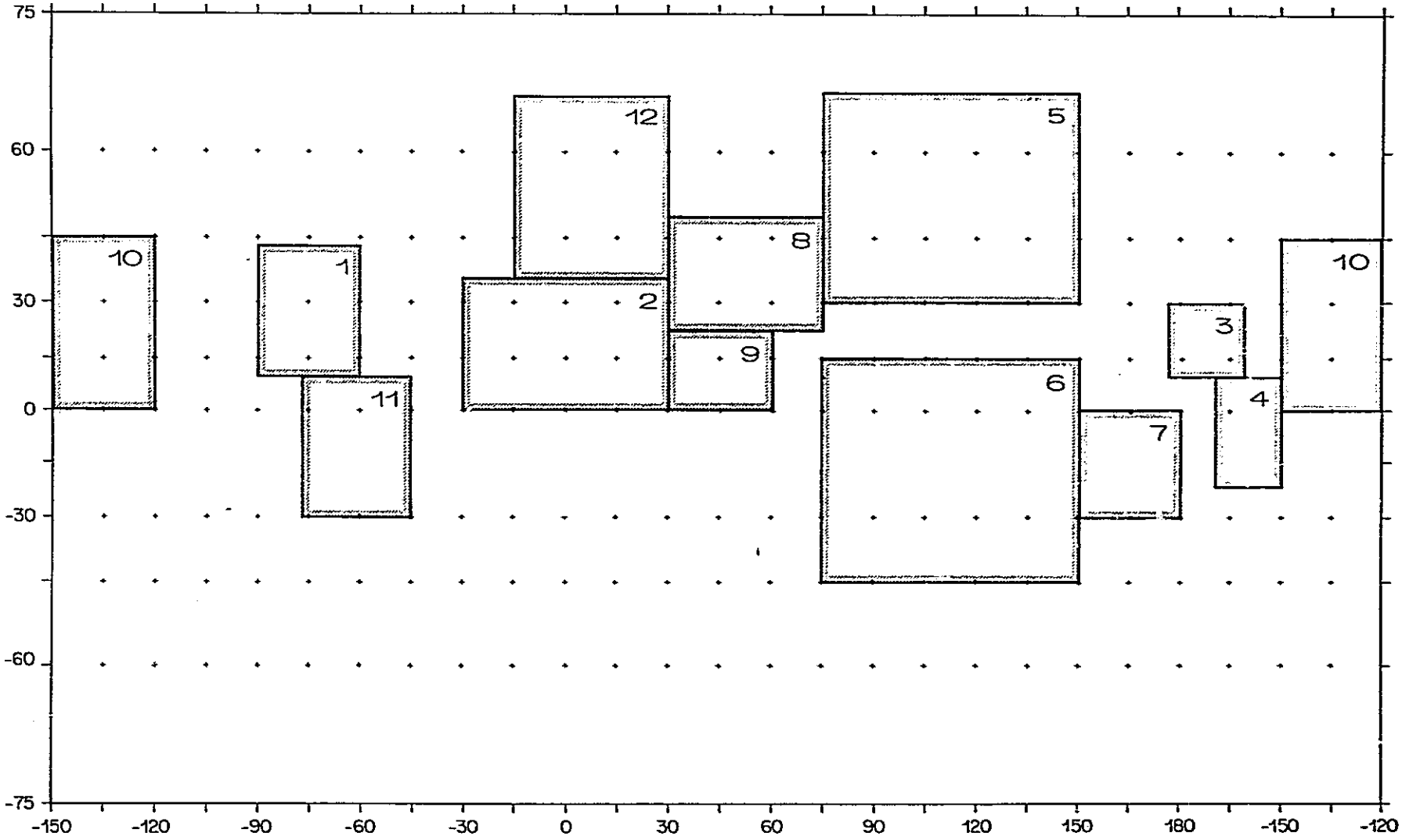

Fig. 13 Areas used for plotting radial gravity at 300km altitude versus topography.

topographic features are plotted in Figure 14. All these regions show positive slopes of gravity to topography. These slopes are an average of the admittance response as a function of wavenumber (McKenzie and Bowin, 1976). The magnitudes for the slopes lie in two groups. One has high slopes of 12 to 18 mgal/km, and the other has lower slopes ranging from 5 to 9 mgal/km. Beta Regio and South Atla both lie within the high slope group, and they also have the largest magnitude positive anomalies in the constant altitude maps. Interestingly, however, Sappho, Eisila and North Atla have slopes intermediate between those for Beta and South Atla, although their maximum gravity values and topographic heights are lower than for those two features. Thus, the mass anomalies of Beta, Sappho, North Atla, and South Atla are greater than would be anticipated from their topographic expression relative to that for Aphrodite and the other features of the low-slope group. These four features with high gravity to topography slopes presumably have a similar explanation, but one that is different from that for the low-slope features.

The continent-sized mass of Aphrodite has a slope of about 9 mgal/Km (Figure 14, area 6); hence it is at the top of the low-slope group, and thus the explanation for its large gravity anomaly could help explain those with lower slopes. A profile across Aphrodite along 85°E at a constant altitude of 380 km was calculated (Figure 15) for comparison with the gravity profile at spacecraft altitude used by Bowin (1983, Figure 14) in analyzing the gravity-topography admittance function for that feature. Note the slight displacement to the south of the maxima for the harmonic spline results, compared to the location of the maxima in the first estimate results at spacecraft altitude obtained by Bowin (1983). This displacement away from the position of perigee confirms that the harmonic spline results compensate for the geometric distortion identified by Bowin (1983, Figure 10) and Gottlieb (1970). The

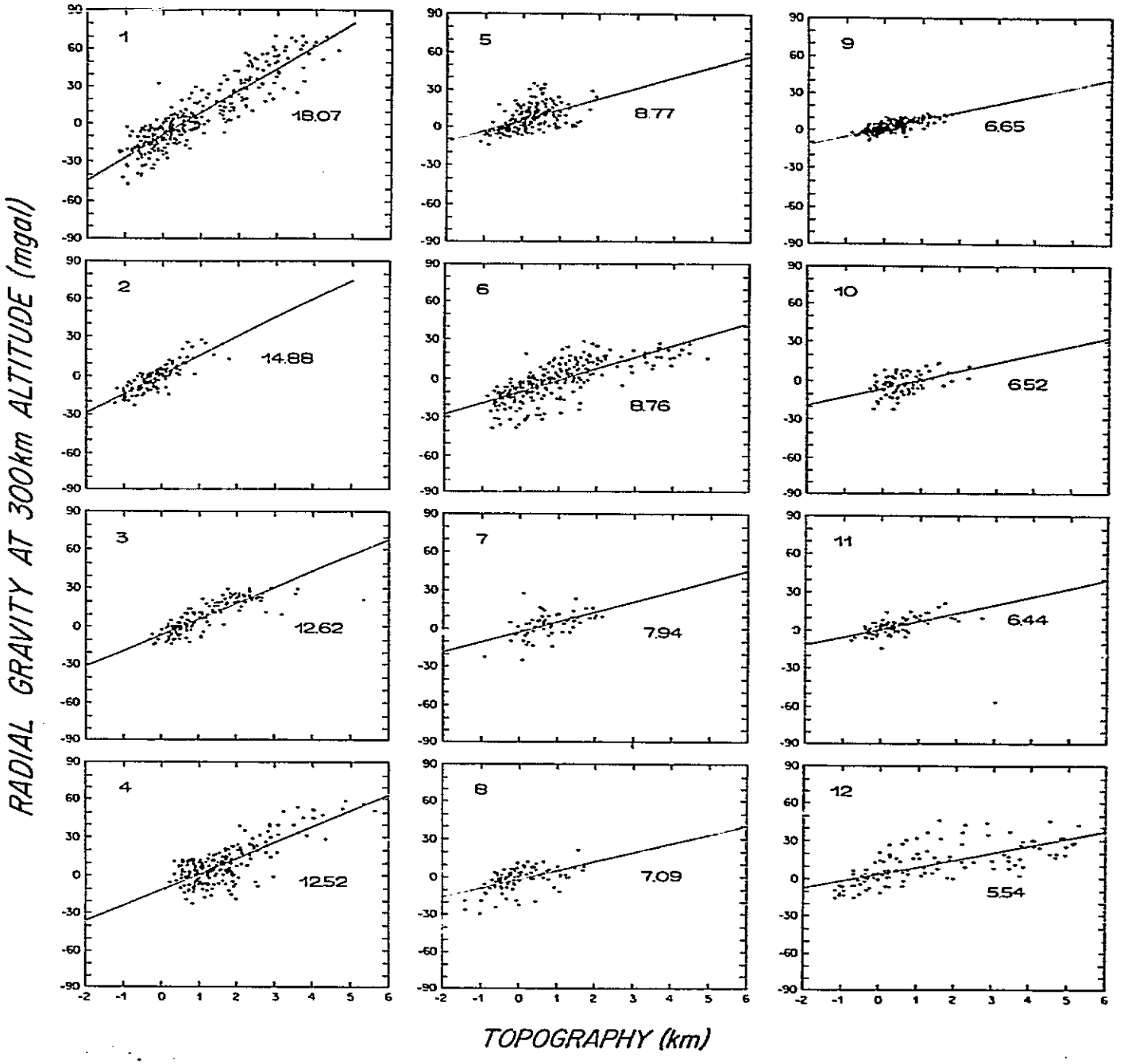

Fig. 14 Radial gravity at 300 km altitude versus topography for areas shown in Figure 11. Plots are numbered in order of decreasing slope values (mgal/km). Areas with the four highest slope values are, 1) Beta Regio, 2) Sappho and Eisila, 3) North Atla, and 4) South Atla.

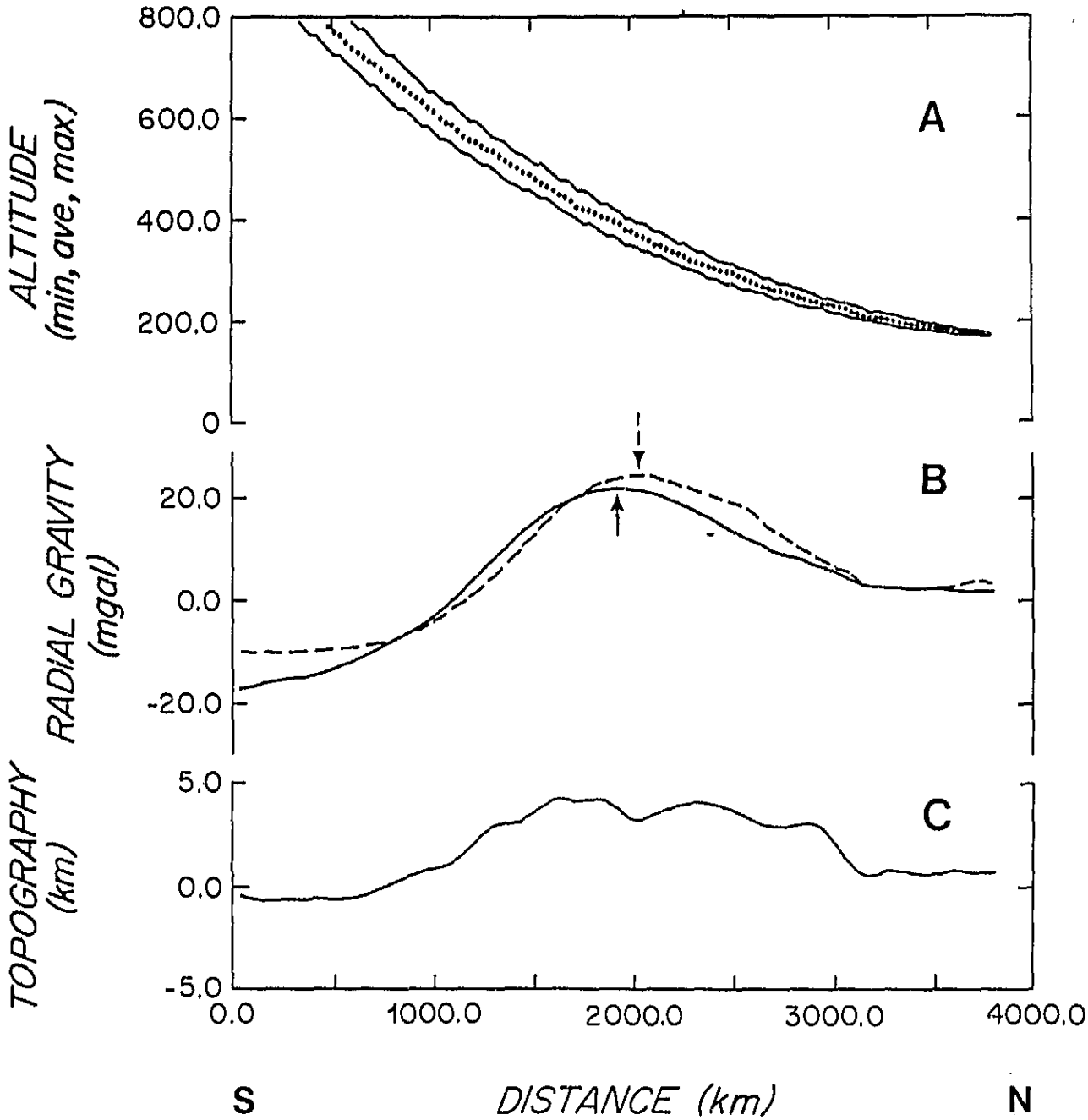

Fig. 15 Profiles across Aphrodite along 85°E. North is to right. Bottom profile shows topography from Pioneer Venus Radar Mapper data. Center profile compares radial gravity (dashed line) estimated by Bowin (1983, Eq. 11) with radial gravity (solid line) estimated by harmonic splines. Arrows indicate displacement of anomaly crest away from peristasis by use of harmonic splines. Uppermost profiles how altitude range of the LOS data. Modified from Bowin (1983, Figure 14).

inference by Bowin (1983, p. 365) that the gravity high near 60°N, 20°W in his first-estimate map would shift northward if geometrically corrected, and would correlate with Ishtar Terra, is also substantiated in the maps of this paper.

The close agreement between the harmonic spline gravity profile at 380 km altitude and the first-estimate vertical gravity profile at spacecraft altitude helps to support the analysis of Aphrodite conducted by Bowin (1983). He convolved elastic plate and Airy isostatic models with the topography along this profile across Aphrodite, and found that, to match the general amplitude of the observed gravity anomaly (about 33 mgal), an elastic plate model would require a plate thickness of about 180 to 200 km, much thicker than that found for earth structures and, because of the high surface temperatures, unlikely for Venus. However, an Airy isostatic model provides a better match between the predicted and observed gravity anomalies if the nominal crustal thickness is about 70 to 80 km, assuming a topographic density of 2800 kg m^{-3}. This thickness is over twice that for continental crust on earth, and considerably greater than that of the earth's basaltic ocean crust (only 5 km). Thus, the larger gravity anomalies that occur on Venus, relative to those on earth for similar sized features, can be explained in the case of Aphrodite by a much thicker basaltic crust on Venus than on earth. The eclogite transition would be expected to be depressed to a greater depth than on earth because of the higher crustal temperatures for Venus, thereby perhaps permitting a greater thickness of basaltic crust to develop. Anderson (1980) suggested that, because of its higher surface temperatures, Venus is likely to have a much thicker basaltic crust than the earth. Phillips et al. (1981) obtained estimated depths of compensation of about 115 km $\pm$30 km for western Aphrodite and two isolated smaller features to the northwest, assuming a combination of local compensation and regional elastic flexure and a density of 3000kg m^{-3}.

However, Phillips et al. (1981) argue against long-term passive (isostatic) compensation at 100 km depth by elastic flexure, and also against compensation occurring at the crust-mantle boundary. They infer instead that the highlands may be dynamically supported by convection in the mantle. Because gravity anomalies at spacecraft altitude even correlate with small topographic features, and presuming there is crust-mantle boundary at some depth, we consider the gravity-topography relations to provide the best estimate of its depth (70 to 80 km).

What then is the origin for the features of the high-slope group? Their greater slope might indicate that they have a greater depth of local compensation as inferred by Sjogren et al. (1983), and estimated at 330 km by Esposito et al. (1982) for the Beta region. This depth is substantially greater than that estimated for Aphrodite and, by inference from the distribution of the low-slope group, for most of the planet. Reasenberg et al. (1982, Figure 3) determined an estimate of the spectral admittance function of gravity to topography in the region of Beta Regio. Their determined function is not smooth, but it strongly suggests that neither a single Airy nor elastic flexure compensation model can satisfy the data. They suggest that at least two mechanisms are required, perhaps deep compensation or dynamic support for Beta Regio and more shallow compensation for other features in the vicinity. The deep compensation perhaps arises from thermal expansion of the mantle caused by a hot plume-like intrusion beneath Beta Regio. Upon dissipation of the thermal anomaly, its contribution to a higher gravity admittance would also decay, thus suggesting a young age for such features.

Another possible explanation, which we consider likely, also leads to the assumption that the features of the high-slope group are younger than the rest of the positive topographic features. A viscous relaxation response to new

surface loads, from recent eruptions, for example, would result in the crust temporarily sustaining a greater load than at eventual equilibrium. During that time, those features would have higher admittance relations than for features that previously attained isostatic equilibrium. Lightning in the vicinity of Beta Regio and south Atla suggests that they are volcanic constructs presently active (Bowin, 1983), as possibly do the recent variations in the abundance of atmospheric sulfur dioxide (Esposito, 1984). A combination of broad surface uplift from thermal expansion at depth and recent volcanic surface loading may explain the high gravity anomalies observed at Beta Regio and south Atla.

MARS: APPLICATION OF THE METHOD OF HARMONIC SPLINES

Figure 16 is a color map of the gravity field of Mars at 300 km altitude obtained from a recent harmonic spline model. The largest magnitude gravity anomalies on Mars are associated with the volcanoes Olympus Mons, Ascraeus Mons, Pavonis Mons, and Arsia Mons. The gravitational effects of the last two appear to be combined into a single anomaly feature in Figure 16. The large elongate lows extending north and south of Olympus Mons are interpreted to be artifacts of the least squares filtering applied during the orbit determination processing from which the residual Doppler LOS acceleration vectors resulted. Downward continuation of these artifacts to produce the constant altitude gravity maps dramatizes these errors. This was first noted in the gravity maps for Venus at constant altitude (Bowin et al., in press) for the Beta Regio feature. For Venus this effect is particularly obvious because the LOS data at any location are concentrated in a narrow zone of altitudes. LOS data for Mars and the moon are available from several different altitudes, and the harmonic spline model tries to produce the smoothest model that will

ORIGINAL PAGE
COLOR PHOTOGRAPH

Fig. 16 Mars Radial Gravity at 300 km altitude above surface. Contour interval is 10 milligal.

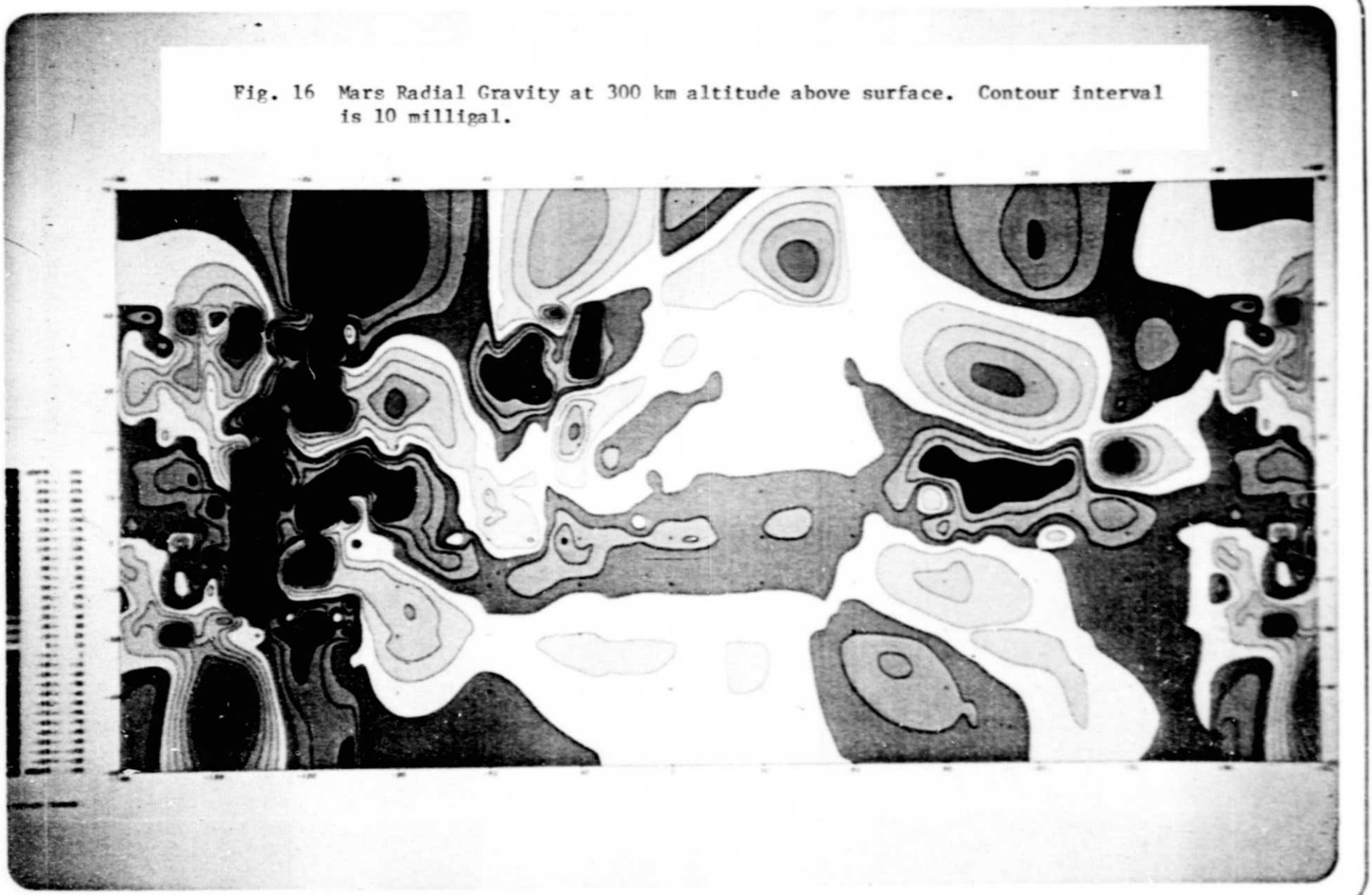

fit the data at all heights, thus lessening the anomaly that would otherwise have come from downward continuing a model that only matched to the highest altitude LOS data.

Positive gravity anomalies are also associated with Alba Patera and Ellysium Mons, and negative gravity anomalies are associated with Valles Marineris, Margaritifer Sinus, Sinus Meridiani, Sinus Sabaeus, Syrtis Major Planitia, Isidis Plantia, and southern Utopia Planitia. Several other positive and negative gravity anomalies occur, but do not appear to be related to obvious surficial features.

MOON: APPLICATION OF THE METHOD OF HARMONIC SPLINES

Figure 17 is a color map of the gravity field of the moon at 50 km altitude obtained from a recent harmonic spline model. The lowering of the surface by 50 km, mentioned in the figure caption, is one of the means by which additional smoothing of the LOS data can be achieved. The data used in constructing this map are from the Apollo 15 and 16 subsatellites and revs of the Apollo 16 and 17 Command modules. Hence these data are restricted to narrow latitude limits both north and south of the equator. The revs that cross the south portion of Mare Imbrium were not available, and thus the mascon of Mare Imbrium is not in evidence in the map, and only the south edge of the Mare Serenitatis mascon is observed. The mascons of Mare Nectaris, Mare Crisium, Mare Smyth II, Mare Humorum, and Mare Orientale are clearly in evidence in the harmonic spline model. Note particularly the circular pattern of high and low gravity anomalies defined for Orientale impact structure. A single harmonic spline solution for the Orientale Region is presented in Figure 18. The outer high corresponds in location with the outer ring of mountains, of which the Cordillera Mountains are in the northeast quadrant.

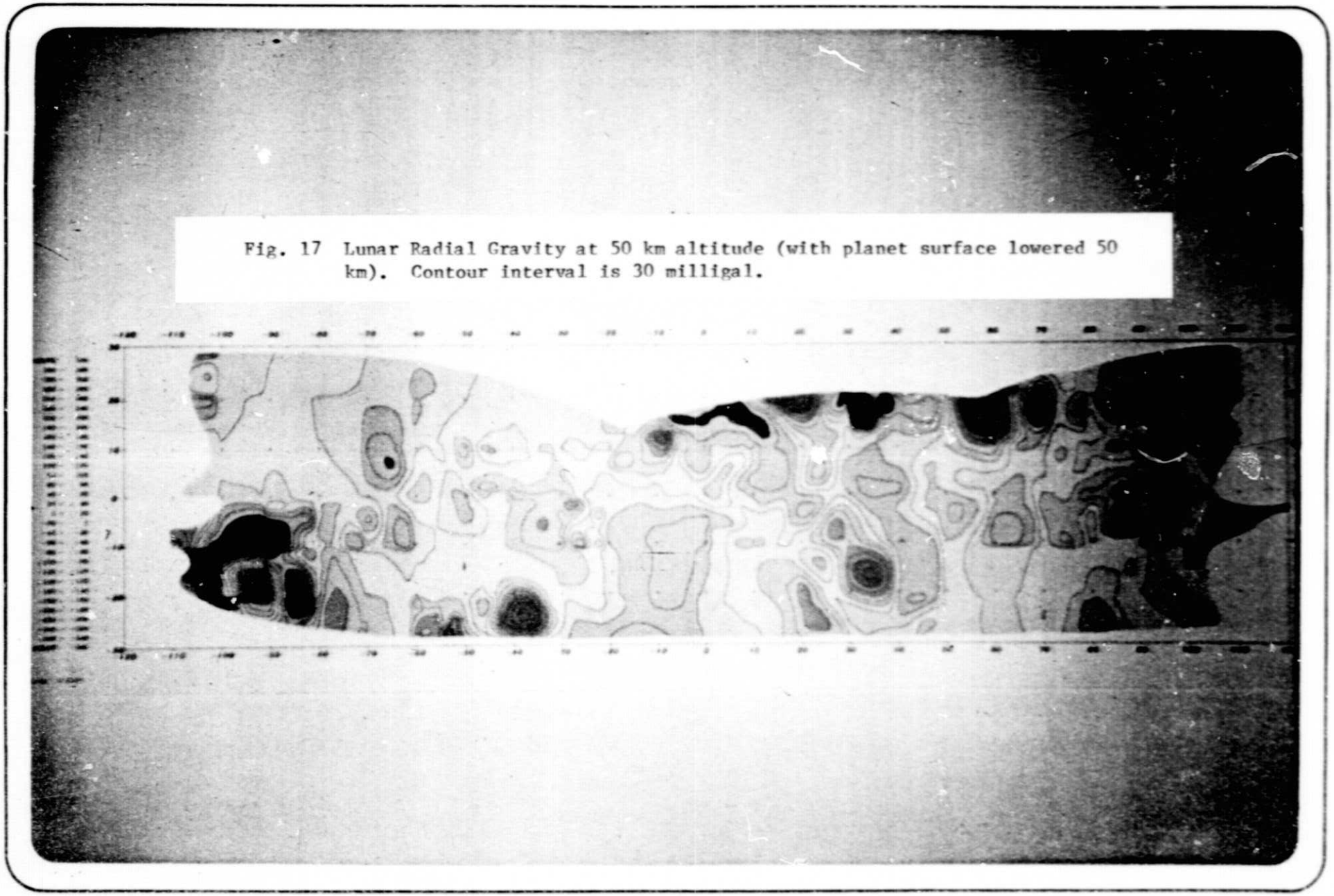

Fig. 17 Lunar Radial Gravity at 50 km altitude (with planet surface lowered 50 km). Contour interval is 30 milligal.

ORIGINAL PAGE
COLOR PHOTOGRAPH

Fig. 18 Radial Gravity Orientale Region of the Moon at 50 km altitude (with planet surface lowered 50 km). Contour interval is 20 milligal.

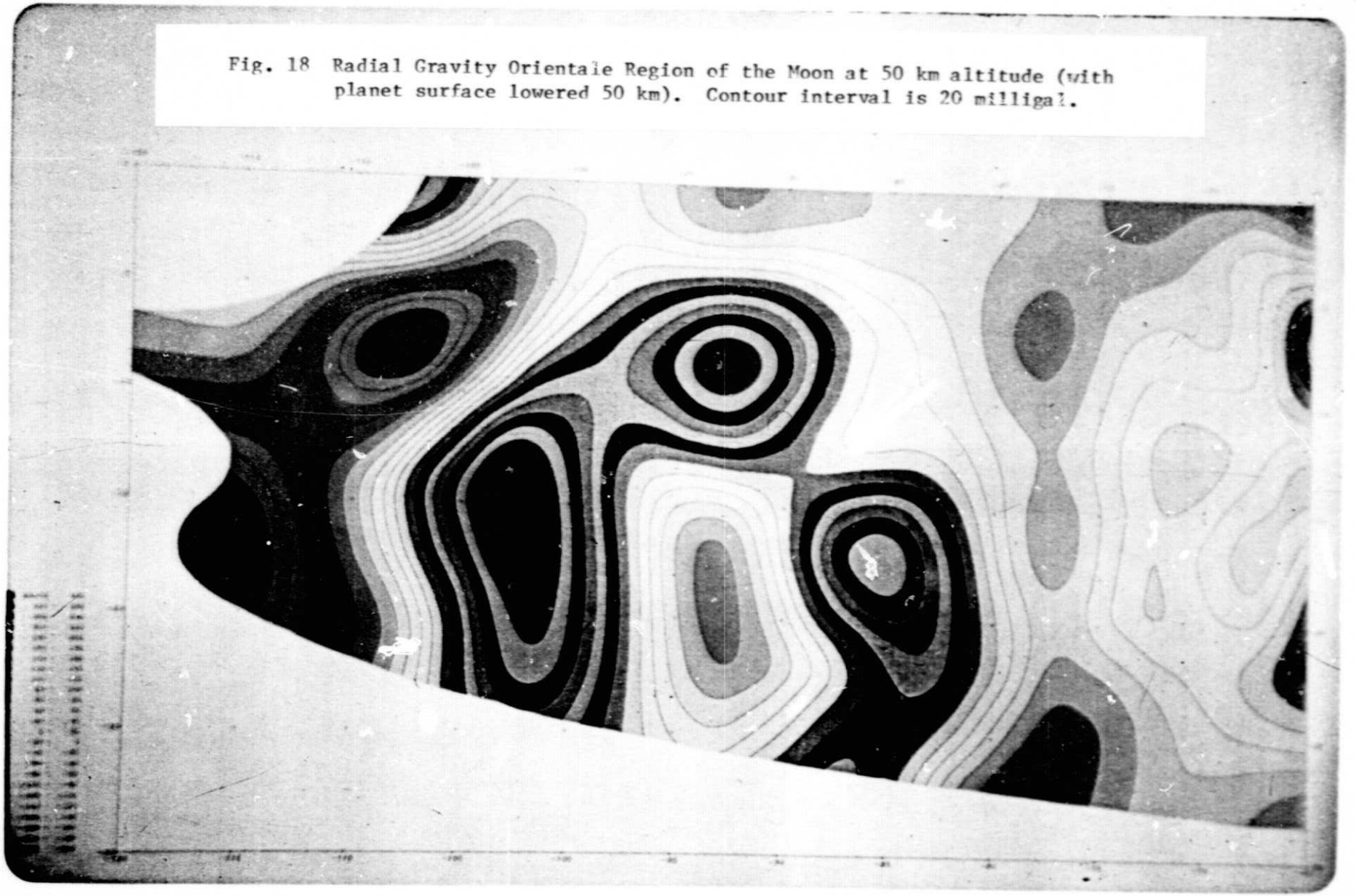

The negative gravity anomaly ring within the outer high corresponds with the location of the Mare Verbis and Mare Pacificus plains. The local lows within the negative ring may be more a function of data distribution than of heterogeneity of structure. The inner positive gravity anomaly high is the mascon of the inner volcanic flooding of Mare Orientale itself.

CONCEPTION OF METHOD FOR OBTAINING ESTIMATES OF TRUE GRAVITY ANOMALIES FOR VENUS, MARS, AND THE MOON

At the end of this contract period we realized that corrections for errors in the zero reference level produced by the least squares filtering procedure are now possible. We submitted a proposal to NASA to use the harmonic spline gravity models as input to the ORBSIM program, produced by JPL, and compute the expected distorted LOS vectors that would result if the harmonic spline model were the actual field. The ORBSIM program allows computed values along an orbit path to be integrated along that orbit path to produce distortion of the model's gravity field like that distorting the LOS vector values. This procedure is described by Phillips et al. (1978) for previous analyses using point and disk mass models. The difference between the simulated LOS vectors and the observed LOS vectors would then be used to calculate modified LOS vectors. A harmonic spline model would then be computed again from the modified LOS vectors. The process is then repeated: use ORBSIM to compute distorted LOS vectors from the new harmonic spline model and compare with the original LOS vectors. Using the difference, modify the observed LOS vectors and recompute another harmonic spline model from the modified LOS values. The original LOS vectors, of course, are retained unblemished for comparison with ORBSIM results of each new model. Iterate until satisfactory convergence is achieved; the resulting harmonic spline model should then represent a close

approximation to the actual anomalous gravity field of the planet, and its distorted product should match the LOS vectors! A variant of this procedure, which presumably may permit a faster convergence, is to compute harmonic spline solutions for the difference vectors (between simulated and observed LOS vectors), and to use those models to estimate the distortion. New calculated distorted LOS vectors would then be computed from the combination of the distortion harmonic spline model and the original harmonic spline model. This process would then be iterated to satisfactory convergence. We proposed to use these methods first with the Pioneer Venus LOS data which has orbits restricted to a narrow range of altitude as a function of latitude, and for which the gravity anomalies are so clearly related to surficial topographic features. The LOS data for Venus, also, is of high quality. We proposed to use the harmonic spline model for Venus (Bowin, et al., submitted) as the starting model. Assuming this procedure is successful for Venus, we would then similarly process the harmonic spline models for Mars and the moon. The resulting harmonic spline gravity fields can then be used directly for analysis and comparison with gravity anomalies computed from structure models for surface features. Although we see no flaw in this proposed method, the proposal was declined. We have documented and submitted to the Discipline Scientist our reasons for concluding that the cited reasons for the declination are unsubstantial, and presently await a reply.

REFERENCES CITED

Ananda, M.P., W.L. Sjogren, R.J. Phillips, R.N. Wimberly, and B.G. Bills, A low-order gravity field of Venus and dynamical implications. J. Geophys. Res., 85, 8303-8318, 1980.

Anderson, D.L., Tectonics and Composition of Venus. Geophys. Res. Letters, 7, No. 1, 101-102, 1980.

Balmino, G., K. Lambeck, and W.M. Kaula, A spherical harmonic analysis of the earth's topography. J. Geophys. Res., 78, (2), 478-481, 1973.

Bills, B.G., Venus: topography, gravity and resonant rotation. EOS, 63, (45), 1021, 1982.

Bowin, C.O., Depth of principal mass anomalies contributing to the earth's geoidal undulations and gravity anomalies. Mar. Geodesy, 7, 61-100, 1983a.

Bowin, C.O., Global gravity maps and the structure of the earth, In: The Utility of Regional Gravity and Magnetic Anomaly Maps (SEG), in press.

Bowin, C.O., Gravity, topography and crustal evolution of Venus. Icarus, 56, 345-371, 1983

Bowin, Carl, G.A. Abers and Loren Shure, 1983 (submitted). Gravity Field at Constant Altitude and Comparison with Earth. Proceedings of the 15th Lunar and Planetary Science Conference.

Bowin, C.O., W. Warsi, and J.Milligan, Free-air gravity anomaly map and Atlas of the World. Geol. Sci. Am. Map and Chart Series, MC-45 and MC-46, 1982.

Bretherton, F.P., R.E. Davis, and C.B. Fandry, A technique for objective analysis and design of oceanographic experiments applied to MODE-73. Deep Sea Res., 23, 559-582, 1976.

Esposito, L.W., Sulfur dioxide: episodic injection shows evidence for active Venus volcanism. Science, 223, 1072-1074, 1984.

Esposito, P.B., W.L. Sjogren, N.A. Mottinger, B.G. Bills, and E. Abbott, Venus gravity: analysis of Beta Regio. Icarus, 51, 448-459, 1982.

Gandin, L.S., Objective Analysis of Meteorological Fields. Israel Program for Scientific Translations, 1965.

Gottlieb, Peter, Estimation of local lunar gravity features. Radio Sci., 5 (2), 301-312, 1970.

Jackson, J.D., Classical Electrodynamics. Wiley, New York, N.Y., 1962.

Jordan, S.K., Statistical model for gravity, topography, and density contrasts in the earth. J. Geophys. Res., 83, 1816-1824, 1978.

Lee, W.H.K. and W.M. Kaula, A spherical harmonic analysis of the earth's topography. J. Geophys. Res., 72, No. 2, 753-758, 1967.

Lerch, F.J., S.M. Klosko, R.E. Laubscher, and C.A. Wagner, Gravity model improvement using Geos 3 (GEM 9 and 10). J. Geophys. Res., 84, 3897-3916, 1979.

Lerch, F.J., S.M. Klosko, and G.B. Patel, A refined gravity model from Lagoes (GEM-L2). Geophys. Res. Letters, 9, No. 11, 1263-1266, 1982.

McKenzie, D.P. and C.O. Bowin, 1976. The relationship between bathymetry and gravity in the Atlantic Ocean. J. Geophys. Res., 81, (11), 1903-1915.

Mottinger, N.A., W.L. Sjogren, G.B.Trager, and B.G. Bills, Venus: 10th degree and order global gravity field (abst.). EOS Transactions, Amer. Geophys. Union, 64, No. 45, 1983.

Parker, R.L. and L. Shure, Efficient modeling of the earth's magnetic field with harmonic splines. GRL 9, No. 8, 812-815, 1982.

Pettingill, G.H. and P. Ford (personal communication).

Phillips, R.J., W.M. Kaula, G.E. McGill, and M.C. Malin, Tectonics and Evolution of Venus. Science, 212, No. 4497, 879-887, 1981.

Phillips, R.J., W.L. Sjogren and E.A. Abbott, Simulation Gravity Modeling to Spacecraft-Tracking Data: Analysis and Application. J. Geophys. Res., 83, 5455-5464, 1978.

Phillips, R.J., J.E. Conel, E.A. Abbot, W.L. Sjogren, and J.B. Morton, Mascons: Progress toward a unique solution for mass distribution. J. Geophys. Res., 77, 7106-7114, 1972.

Reasenberg, R.D, Z.M. Goldberg, P.E. MacNeil, and I.I. Shapiro, Venus gravity: a high-resolution map. J. Geophys. Union, 86, No. B8, 7173-7179, 1981.

Reasenberg, R.D., Z.M. Goldberg, and I.I. Shapiro, Venus: comparison of gravity and topography in the vicinity of Beta Regio. Geophys. Res. Letters, 9, No. 6, 637-640, 1982.

Shure, L., R.L. Parker, and G.E. Backus, Harmonic splines for geomagnetic modeling. PEPI, 28, 215-229, 1982.

Shure, L., K. Whaler, D. Gubbins, and B. Hobbs, Physical constraints for the analysis of the geomagnetic secular variation. PEPI, 32, 114-131, 1983.

Sjogren, W.L., B.G. Bills, P.W. Birkeland, P.B. Esposito, A.R. Konopliv, N.A. Mottinger, S.J. Ritke, and R.J. Phillips, Venus gravity anomalies and their correlations with topography.. J. Geophys. Res., 88, No. B2, 1119-1128, 1983.

Sjogren, W.L., P.W. Birkeland, P.B. Esposito, R.N. Wimberly, and S.J. Ritke, Venus gravity field: Local. Trans. Amer. Geophys. Union, 61 (17), 386, 1981.

Sjogren, W.L., R.J. Phillips, P.W. Birkeland, and R.N. Wimberly, Gravity anomalies on Venus. J. Geophys. Res., 85, No. A13, 8295-83021, 1980.

Williams, B.G., N.A. Mottinger, and N.D. Panagiotacopulous, Venus gravity field: pioneer Venus orbiter navigation results, Icarus, 56, 578-589, 1983.